Volume 4

Chapter 11

https://doi.org/10.32685/pub.esp.38.2019.11
Published online 14 May 2020

Subduction Geometries in Northwestern South America

Carlos Alberto VARGAS[1]*

1 cavargasj@unal.edu.co
Universidad Nacional de Colombia
Sede Bogotá
Departamento de Geociencias
Carrera 30 n.° 45–03
Bogotá, Colombia

* Corresponding author

Abstract Using hypocentral solutions and arrival times of first P and S waves recorded by stations of the Red Sismológica Nacional de Colombia (RSNC), as well as GPS, gravity, and magnetic public datasets, I have estimated velocity tomograms, Curie depth points, and the strain field along NW South America to evaluate the subduction process and interactions of the first–order tectonic blocks. A wire model has been estimated supported by three profiles based on gravity forward modeling, earthquake distribution, and b–values to elucidate the subduction behavior of the Caribbean and Nazca Plates under the South America Plate, highlighting at least three subduction scenarios, where in addition to the Caldas lithospheric tear, other minor tears are found in the lithospheric system of this region. Although it is possible a flat subduction along NW Venezuela, it is presented as an alternative hypothesis a steeper subduction, which mechanically is coherent with the structural features observed in this region. The wire model shows how the Caribbean Plate accommodates mechanically to change from flat subduction in the south to steeper subduction in the north, differentially uplifting the Santa Marta and Santander Massifs along a weakness zone that corresponds to the Santa Marta–Bucaramanga Fault System. The absence of a modern volcanic arc in the Eastern Cordillera and/or the serranía de Perijá is a consequence of slow low–angle subduction, which is associated with the compressional regime induced by the Panamá tectonic indenter. In this scenario, I hypothesize the presence of a zone of fluid accumulation (>130 km depth) derived from the dehydration process; these fluids cannot ascend to the surface, which impedes the formation of current active magmatism. However, during the last 9–12 Ma of relevant influence of the Panamá Arc against NW South America, other emplacements of magmatic material might have occurred along this orogenic system. The wire model also shows that the low seismic activity within the Antioquian Batholith is a consequence of its rigidity, promoting the transfer of strain derived from the subduction process from west to east, generating high seismic activity along its borders and suggesting that compositional and elastic properties at depth maintain its coherence as a structural body beyond the upper crust. A similar interpretation is indicated for the southern Eastern Cordillera.

Keywords: *local earthquake tomography, Curie point depth, strain field, subduction, Caribbean Plate, Nazca Plate.*

Resumen Usando soluciones hipocentrales y los tiempos de arribo de las primeras ondas P y S registradas por las estaciones de la Red Sismológica Nacional de Colombia (RSNC), así como bases de datos públicas de GPS, gravimetría y magnetometría, se han

Citation: Vargas, C.A. 2020. Subduction geometries in northwestern South America. In: Gómez, J. & Pinilla–Pachon, A.O. (editors), The Geology of Colombia, Volume 4 Quaternary. Servicio Geológico Colombiano, Publicaciones Geológicas Especiales 38, p. 397–422. Bogotá. https://doi.org/10.32685/pub.esp.38.2019.11

estimado tomogramas de anomalías de velocidad sísmica, la profundidad del punto de Curie y el campo de esfuerzos a lo largo del costado noroccidental de Suramérica para evaluar el proceso de subducción y las interacciones de los bloques tectónicos de primer orden. Se ha estimado un modelo soportado por tres perfiles basados en el modelado gravimétrico directo, la distribución de sismos y los valores *b* para dilucidar el comportamiento de la subducción de las placas del Caribe y de Nazca bajo la Placa de Suramérica. Se destacan al menos tres escenarios de subducción, donde además del desgarre litosférico de Caldas, otros desgarres menores se encuentran en el sistema litosférico de esta región. Aunque es posible una subducción horizontal a lo largo del borde noroccidental de Venezuela, se presenta como hipótesis alternativa una subducción más inclinada que mecánicamente es coherente con los rasgos estructurales observados en esta región. El modelo muestra como la Placa del Caribe se acomoda mecánicamente para cambiar de una subducción plana en el sur a una más inclinada en el norte, elevando diferencialmente los macizos de Santa Marta y Santander a lo largo de una zona de debilidad que corresponde al Sistema de Fallas Santa Marta–Bucaramanga. La ausencia de un arco volcánico moderno en la cordillera Oriental o en la serranía de Perijá es una consecuencia de la subducción lenta de bajo ángulo, que está asociada con el régimen compresional inducido por el empuje tectónico de Panamá. En este escenario se asume la presencia de una zona de acumulación de fluidos (>130 km de profundidad) derivados del proceso de deshidratación; estos fluidos no pueden ascender a la superficie, lo que impide la formación del magmatismo activo en la actualidad. Sin embargo, durante los últimos 9–12 Ma de importante influencia del Arco de Panamá contra Suramérica, otros emplazamientos de material magmático podrían haber ocurrido a lo largo de este sistema orogénico. El modelo también muestra que la baja actividad sísmica en el Batolito de Antioquia es una consecuencia de su rigidez, lo que fomenta la transferencia de deformación derivada de los procesos de subducción de occidente a oriente y genera una alta actividad sísmica a lo largo de sus bordes. Esto sugiere que las propiedades composicionales y elásticas a profundidad mantienen su coherencia como un cuerpo estructural más allá de la corteza superior. Una interpretación similar es indicada para el sur de la cordillera Oriental.

Palabras clave: *tomografía sísmica local, profundidad del punto de Curie, campo de esfuerzo, subducción, Placa del Caribe, Placa de Nazca.*

1. Introduction

The subduction of different bathymetric relief drives changes in the kinematics and dynamics of convergence zones (Rosenbaum & Mo, 2011). These authors suggest that the buoyancy of high bathymetric relief flattens the dip of the subducting slab, modifying the structural and magmatic evolution of the overriding plate and volcanic arcs and the retreating plate boundaries that can inhibit subduction rollback, a process that may locally pin the subduction hinge and lead to the progress of cusps and slab tearing. Other authors suggest that sometimes subduction rollback is annulated by flat subduction (see, e.g., Horton, 2018). In any case, a brief inspection of the bathymetric relief of the Pacific Ocean and Caribbean Sea around NW South America (Figure 1) allows the identification of contrasting conditions of relief that, in addition to the age and converging velocity of the slabs (see, e.g., Carrillo et al., 2016; Cediel et al., 2003; Gutscher & Westbrook, 2009; Trenkamp et al., 2002), promote a broad variety of subduction styles along ca. 2000 km in both margins. In addition, it is thought that the north Andes morphology is the result of the interaction at depth of the Nazca and Caribbean Plates under NW South America (Mora et al., 2015; Taboada et al., 2000), where a broad orogen to the south splits into three cordilleras northward with changes in direction, composition, and dominant age, as well as structural styles (Parra et al., 2012; Reyes–Harker et al., 2015). These changes result in a complex lithospheric system.

In this sense and during the last three decades, several studies have proposed complicated interactions between these three lithospheric plates and other tectonic blocks along this region (see, e.g., Cortés & Angelier, 2005; Lara et al. 2013; Taboada et al., 2000). However, despite several tomographic studies of velocity and attenuation in 2D and 3D, derived from observations of arrival times, as well as energy decay in waveforms of local and regional earthquakes (Bernal–Olaya et al., 2015; Chiarabba et al., 2016; Syracuse et al., 2016; van der Hilst &

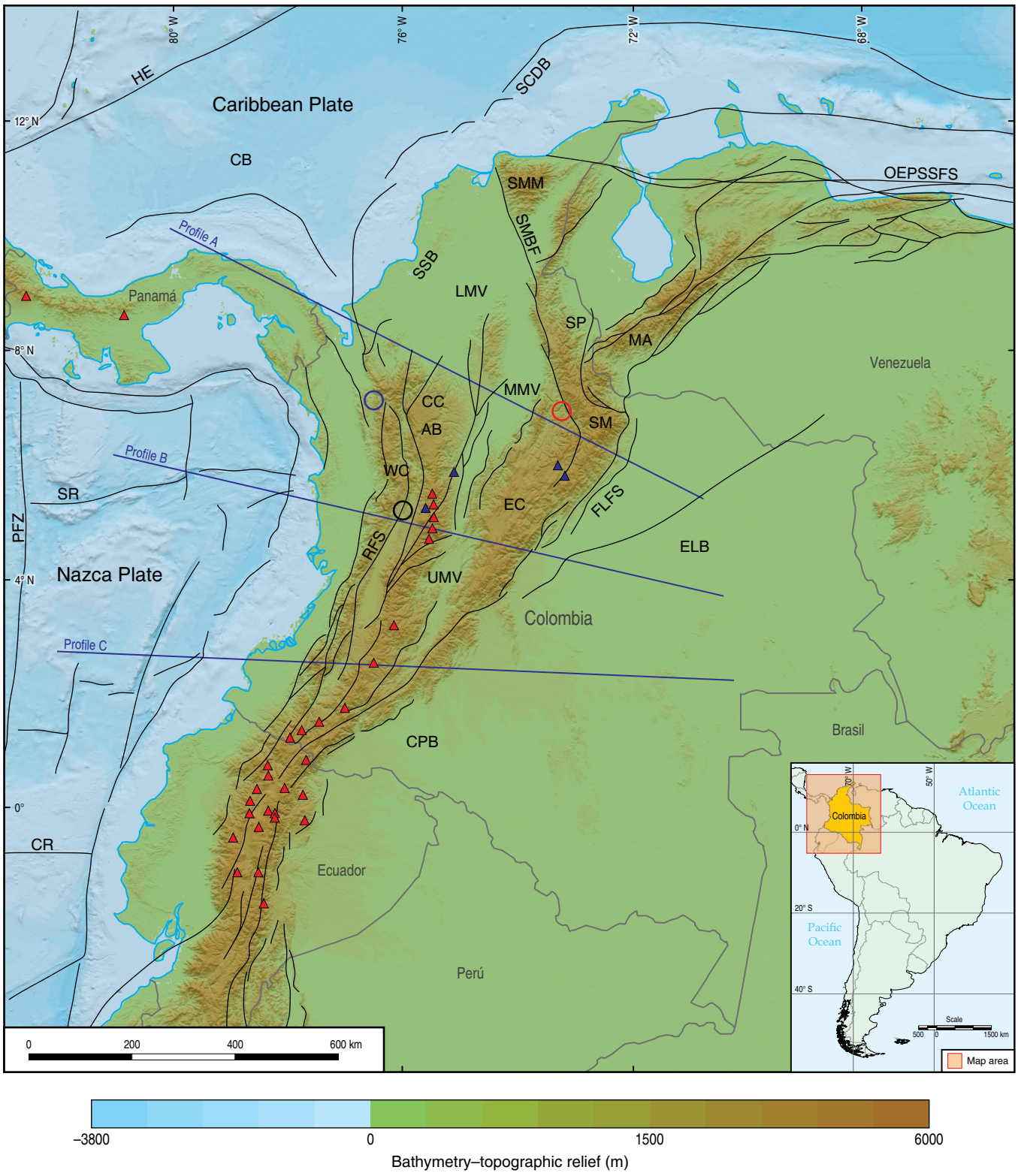

Figure 1. Tectonic features of NW South America, SW of the Caribbean Basin, and east of the Panamá Basin. Shorelines are presented as bold blue lines. Bathymetric–topographic relief with the main tectonic features. (HE) Hess Escarpment; (SCDB) south Caribbean deformed belt; (CB) Colombian Basin; (SMM) Santa Marta Massif; (OEPSSFS) Oca–El Pilar–San Sebastian Fault System; (SSB) Sinú–San Jacinto Basin; (SMBF) Santa Marta–Bucaramanga Fault System; (LMV) Lower Magdalena Valley Basin; (SP) serranía de Perijá; (MA) Mérida Andes; (CC) Central Cordillera; (MMV) Middle Magdalena Valley Basin; (PFZ) Panamá fracture zone; (SR) Sandra Ridge; (WC) Western Cordillera; (AB) Antioquian Batholith; (SM) Santander Massif; (RFS) Romeral Fault System; (EC) Eastern Cordillera; (FLFS) Frontal Llano Fault System; (UMV) Upper Magdalena Valley Basin; (ELB) Eastern Llanos Basin; (CPB) Caguán–Putumayo Basin; (CR) Carnegie Ridge. Red triangles: Active volcanoes; Blue triangles: Inactive volcanoes; Red circle: Bucaramanga nest; Blue circle: Murindó nest; Black circle: Cauca nest.

Mann, 1994; Vargas & Mann, 2013; Vargas et al., 2004;), there are still many doubts about the geometry of the primary tectonic structures that interact in this region.

However, hypocentral solutions seem to be the most consistent information that allows inference of some aspects of the lithospheric system geometry in this zone (Figure 2). For example, two well–differentiated Wadati–Benioff zones separated by an E–W offset ca. 240 km long have suggested the presence of a lithospheric tear (Caldas Tear) formed by the Panamá Arc indenter since the middle Miocene (Chiarabba et al., 2016; Poveda et al., 2018; Syracuse et al., 2016; Vargas & Mann, 2013). This information also highlights at least three seismic nests at different depths (Figures 1, 2) and broad areas of scarce activity defined by the contrasting seismicity (Figure 3). For the sake of conciliating deep and shallow seismotectonic observations, this paper combines estimation of kinematic deformations, thermal structure, and three 2D sections based on gravity modeling, b–values, and hypocentral solutions to present a proposal on the subduction geometries and their contrasting activity in this region of the world. In the discussion, I present some hypotheses that may contribute to explaining the causality of several tectonic features and answering relevant regional geological questions: for example, how may the Caribbean Plate accommodate mechanically with the Santa Marta and Santander Massifs? What phenomena cause the absence of magmatic arcs along the serranía de Perijá or Mérida range? How may we explain the lack of seismicity inside the Antioquian Batholith or inside the Garzón and Quetame Massifs?

2. Geotectonic Setting

NW South America corresponds to a tectonic mosaic dominated by three lithospheric plates: the Nazca and Caribbean Plates of oceanic origin and the South American Plate, an older and continental plate that kinematically drives the northern Andean Block (Cediel et al., 2003). In proximity to the study area, the Nazca Plate is mainly bounded by the continental margins of Panamá, Colombia, and Ecuador to the north, east, and south, and the Panamá fracture zone (PFZ) to the west. Prominent features within the Nazca Plate include the Sandra, Cocos, and Carnegie Ridges. The formation of the plate was caused by the splitting of the oceanic Farallón Plate in the late Oligocene – early Miocene into the Nazca and Cocos Plates (Colgan et al., 2011; Lonsdale, 2005). Currently, the Nazca Plate is moving eastward relative to South America with seismic activity primarily along the continental margins where focal mechanisms suggest extensional processes in areas proximal to the trench and compressional processes associated with the subduction of the Nazca Plate (Figure 4). There is seismic activity along W–E structures related to the Sandra Ridge, but this activity is less well constrained compared to that of the continental areas.

According to Taboada et al. (2000), the former Nazca and Caribbean Plates have approached NW South America since the Cretaceous, promoting oblique subduction along the W margin. Currently, both plates converge in different directions (Figure 4) at ca. 60 and 20 mm/y, respectively (Veloza et al., 2012), generating a compressive regime in the Andes mountain belt that is undergoing active deformation and uplift. If considering the hypothesis that the Panamá Arc is riding on the Caribbean Plate, then the scarce seismic activity along the south Caribbean deformed belt (SDCB) and some continental areas of NW South America may be a response to the converging movements of this plate that are absorbed partially by brittle–plastic behavior in the upper crust (including sedimentary rocks of the Sinú–San Jacinto and Lower Magdalena Valley Basins; see Figures 2, 4b). The slow convergence velocity of the Caribbean Plate could be related to a flat subduction process up to the Lower Magdalena Valley and an abrupt change in the subduction angle around the Middle Magdalena Valley.

The northern Andes is also a consequence of the repeated interaction between terranes of different affinity, age, and stress regimes that accreted against the continental margin of NW South America, which resulted in three cordilleras with pulses of uplift from the Paleogene (Anderson et al., 2016; Gómez et al., 2003; Parra et al., 2009, 2012; Reyes–Harker et al., 2015) to the present. Crustal activity in these cordilleras (Figures 1, 2, 3, 4) may be related to (Corredor, 2003; Cortés & Angelier, 2005): (i) strain released aseismically and accommodated by folding, fault creeping, and rigid block translation, (ii) accommodation of local differences in orientations of inherited basement assemblies, (iii) local response of basement assemblies to stress regimes, and (iv) syntectonic reorientation and rotation of basement assemblies to accommodate different stress regimes.

3. Data and Methods

With the purpose of inferring the subduction geometry, it is necessary to understand the deformational response at the surface of the lithospheric system, as well as to establish its thermal behavior and seismic activity and to spatially illuminate its elastic structure. Hence, in this work, the problem is addressed by (i) estimating the strain field and relating it to the main tectonic features of the region; (ii) calculating the Curie depth point and extrapolating its tendency to establish possible thermal instabilities in the plates; (iii) evaluating contrasts in seismic activity and fracture regime along the intervening structures; and (iv) estimating the field of velocity anomalies Vp, Vs, and the Vp/Vs ratio and relate it to other geophysical variables (e.g., gravity) to identify the continuity of the lithospheric structures and potential processes that destabilize them, e.g., dehydration and gravitational collapse.

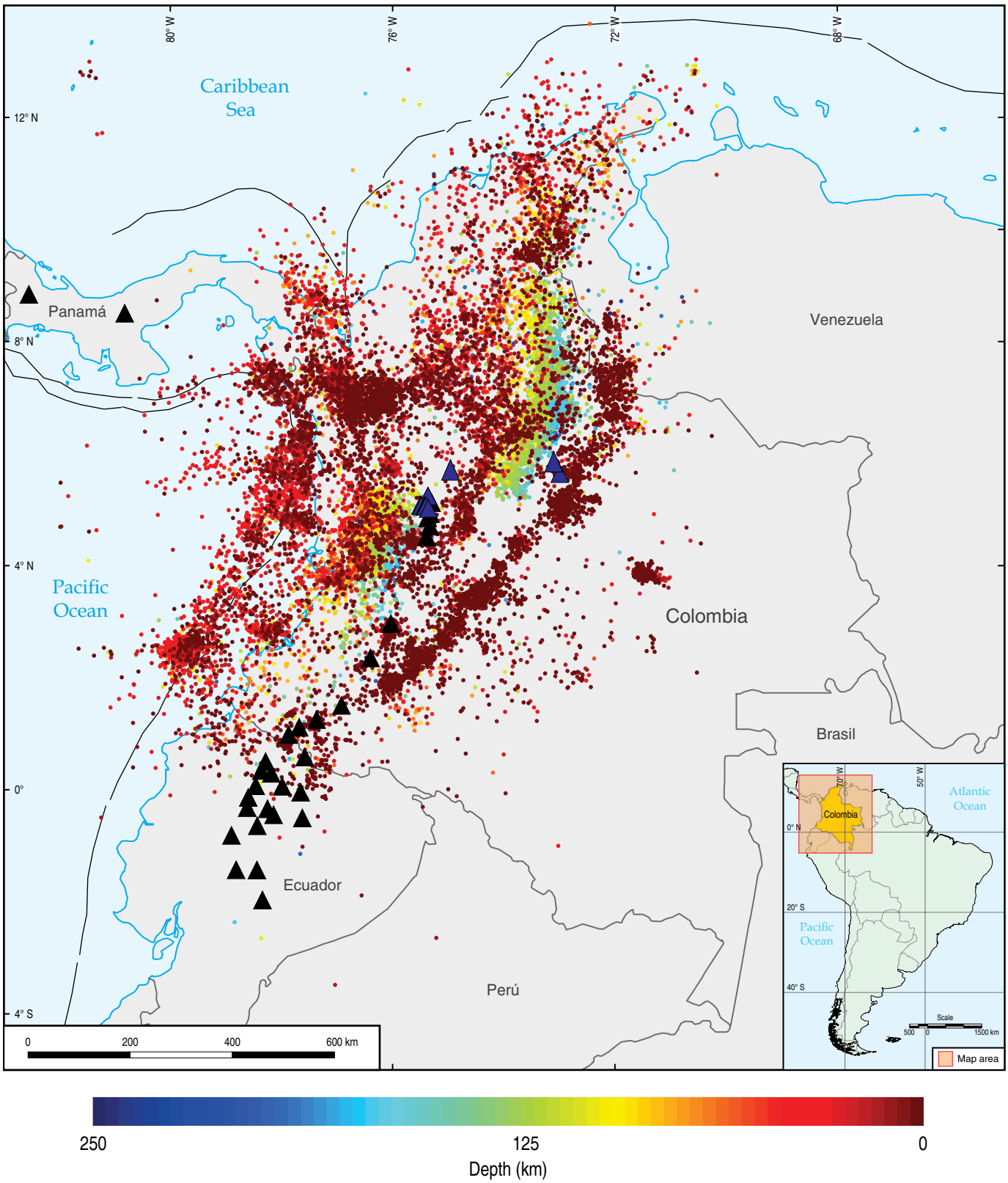

Figure 2. Seismicity of NW South America, SW of the Caribbean Basin, and east of the Panamá Basin. Shorelines are presented as bold blue lines. 166 723 hypocentral solutions calculated by the Red Sismológica Nacional de Colombia (RSNC) from June 1993 to April 2017. The depth distribution of the seismic events marks two well–differentiated Benioff planes (see trends defined by deeper events in yellow dots to blue dots), whose division zone is marked by an inactive volcanic belt with a W–E trend (blue triangles).

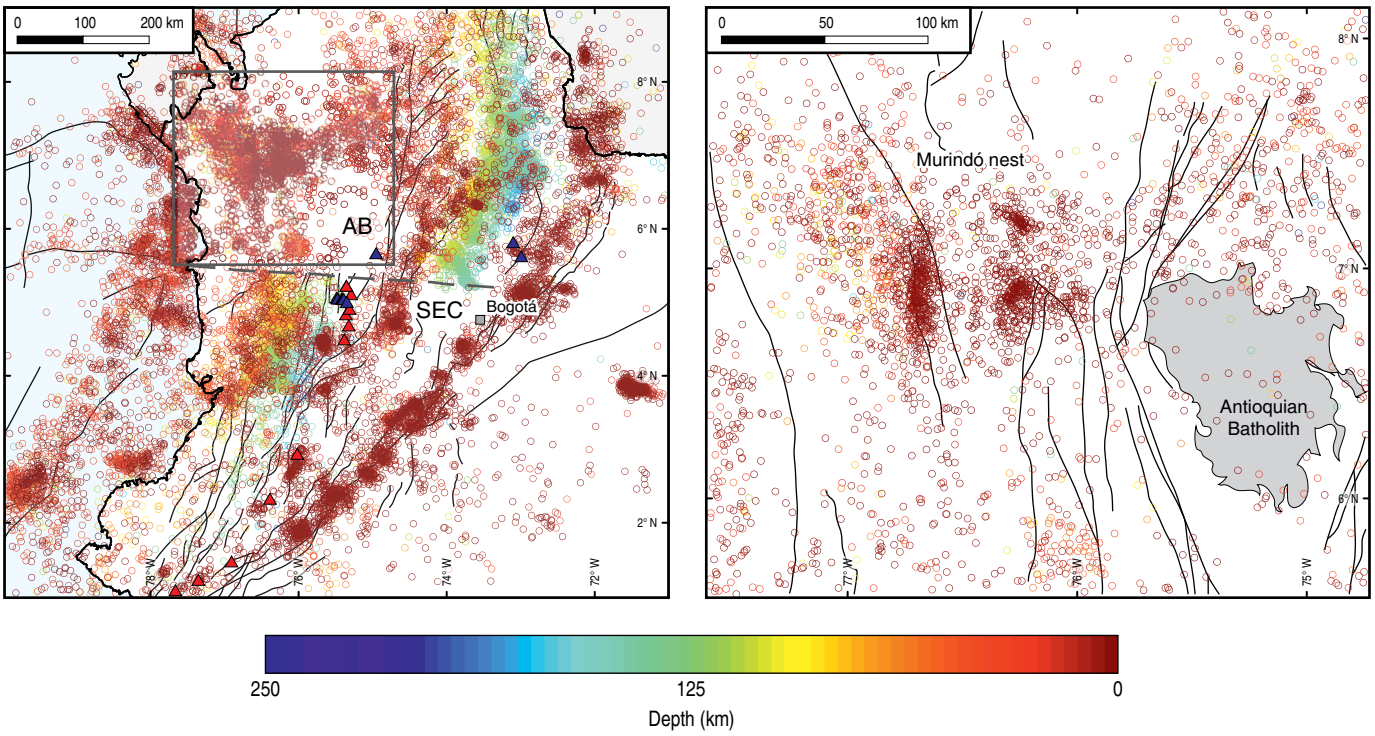

Figure 3. Seismicity of NW Colombia. Shorelines are presented as bold black lines. Map with the distribution of seismicity in the central region of Colombia. (AB) Antioquian Batholith; (SEC) south of the Eastern Cordillera. The dashed gray line represents the Caldas Tear. The gray square indicated the zoomed area on the right side.

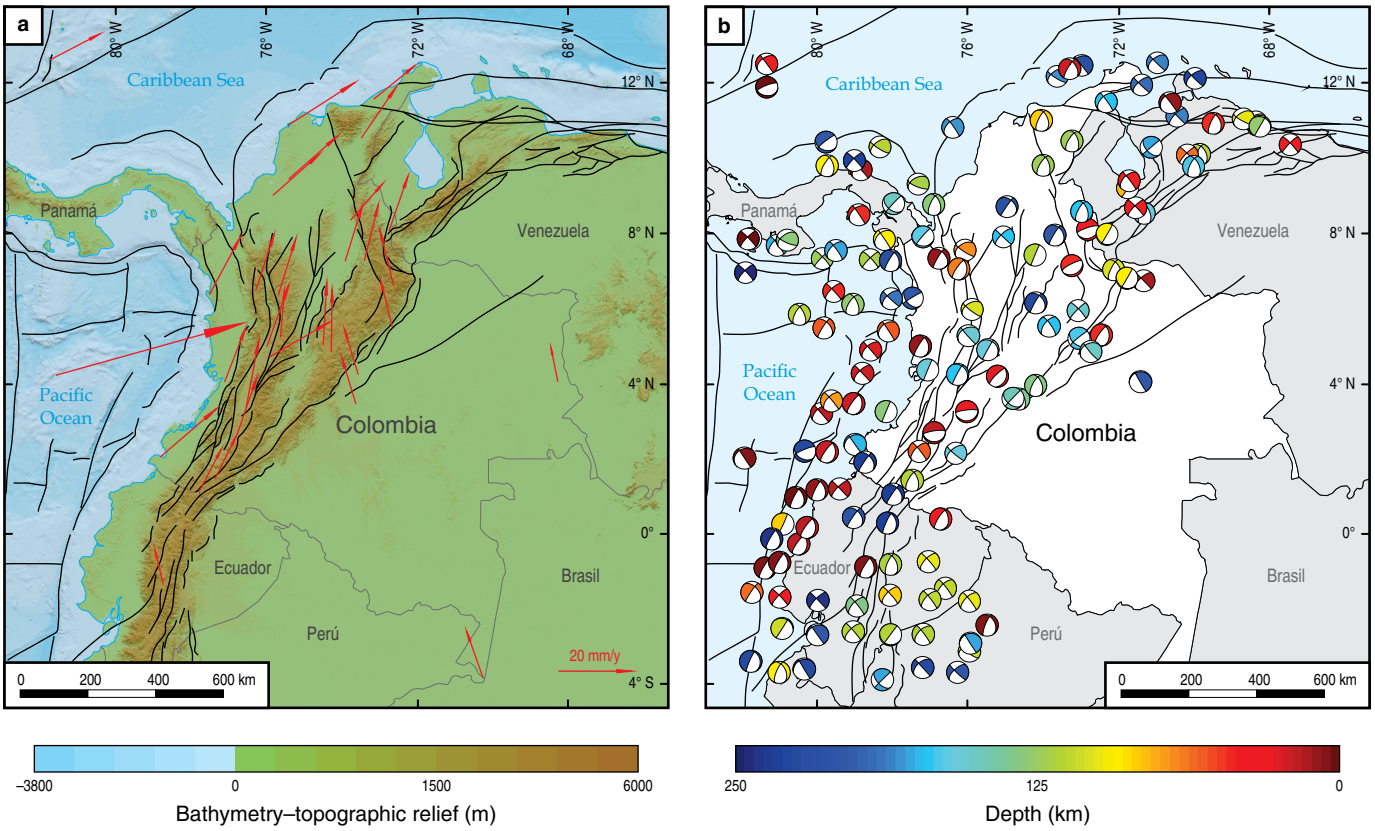

Figure 4. Observations considered for interpreting seismotectonic deformation in NW South America. **(a)** GPS velocity vectors (relative to stable South America) reported by Mora–Páez et al. (2019). **(b)** Focal mechanisms extracted from the global CMT catalog (Ekström et al., 2012).

3.1. Strain Field

The dataset for crustal displacement considered in this study is based on the GPS observations reported by Mora–Páez et al. (2019) and was used to estimate the strain field using the SSPX program (see technical details of the program in Cardozo & Allmendinger, 2009). The program resolves the strain field for this region with 32 stations on the surface in an undeformed (Lagrangian) configuration using a grid–distance weighted spacing of 100 × 100 km. Commonly, spaced deformations highlight the surficial kinematics that may be related to the mantle flux and some aspects of the dynamics of the subduction process.

3.2. Thermal Structure

A typical approach to the thermal structure of the lithospheric system comes from the Curie point depth (CPD) calculations. This parameter represents the depth where the remnant or induced magnetization of minerals in the lithosphere vanishes. This isotherm is presumed to be related to the Curie point of magnetite, which lies between 575 and 585 °C (Hunt et al., 1995). The dataset for this purpose was derived from the World Digital Magnetic Anomaly Map–WDMAM version 2.0 (Dyment et al., 2015, Figure 5a). In this estimation, the presence of a magnetic layer that spreads infinitely and omnidirectionally is assumed (see details in Salazar et al., 2017). The depth to the bottom of this layer is insignificant compared with the horizontal scale of the magnetic source, and its magnetization field can be related to a random spatial function. The numerical calculation of the CPD in this work, which corresponds to approximately the same depth reported by Vargas et al. (2015), is based on the centroid method (Okubo et al., 1985). For the estimations, a rectangular spatial window was selected that ensures a dimensional criterion of six times the depth of the target. Given that the database has a resolution of approximately 5.6 × 5.6 km, the analysis window for each CPD estimate is 336 × 336 km. The window steps 5.6 km in both the x and y directions until the entire area is covered. The uncertainties in the calculations are based on the suggestions by Okubo & Matsunaga (1994).

3.3. The B–value and Seismic Profiles

The Gutenberg–Richter law expresses the linear relationship between magnitudes and the total number of earthquakes in any region and specified time (Lay & Wallace, 1995). The slope of the relationship is known as the b–value and is commonly close to 1.0 in seismically active regions. There is a vigorous debate regarding the proper interpretation of the observed spatial and temporal variations in b–values. Some of the most commonly suggested factors to explain the variations are: (i) stress field; (ii) depth and proximity to the seismic source, and (iii) heterogeneity of the material involved in the fracture and geometry of the fault. However, in this work, the b–parameter may provide information about the activity of plates during the subduction process and the fracture regime in some particular places.

Estimating the b–value used the collected dataset by the Red Sismológica Nacional de Colombia (RSNC) from June 1993 to April 2017. Hypocentral solutions were estimated with the program HYPOCENTER (Ottemöller et al., 2016, SEISAN version 10.5.0), and events were selected with depths ranging between 0 and 250 km, $m_L \geq 1.0$, number of stations used for estimations $N \geq 5$, and RMS time residuals of approximately 1.0 s. Approximately 129 200 solutions met these criteria (Figure 2) and were applied to estimate the spatial distribution of the b–values using the methodology suggested by Wiemer et al. (1998) and the program Zmap (Michael et al., 1990). The same catalog was used to project three vertical sections, each with a corridor 50 km wide (Figure 1), and to calculate the seismic surface that best fits the most frequent and profound events. This coverage derives from averaging all events deeper than 20 km around areas of 50 × 50 km along the study area. The meaning of this surface for some areas may correspond to the brittle–ductile transition zone. Beyond the trench and landward of the continental regions, this surface may represent the Wadati–Benioff topography up to around the volcanic arc.

3.4. 3D Velocity Structure

To estimate the spatial configuration of the lithospheric plates in the study area based on the distribution of velocity anomalies, in this work, first–arrival times of the P and S phases were used. The travel times were measured for 113 269 local earthquakes recorded by 33 seismological stations of the RSNC. The initial hypocentral solutions considered were registered by at least six stations. Both the P and S phases were handpicked. Tomograms associated with the 3D velocity structure were estimated with the LOTOS algorithm for local earthquake tomography (Koulakov, 2009), which performs iterative simultaneous inversions for P and S velocity and source parameters. Vp/Vs values are derived from the independent P and S velocities. A 1D starting model for inverting new hypocentral locations was used (Ojeda & Havskov, 2001). Along the depth levels, the velocity was linearly interpolated. This model was used as the reference starting model for the 3D inversion.

Following Koulakov et al. (2013) and Vargas & Torres (2015), the LOTOS code uses an adaptive mesh parameterization with nodes distributed inside the study volume. There are no nodes in areas with a deficit of ray coverage (less than 10% of average ray density). In final tomograms, the results are masked if the distance to the nearest node is less than a predefined value (50 km in this case). The minimal grid spacing is predefined (20 km in this scenario). To avoid artifacts related to grid orientations, calculations were performed for four different

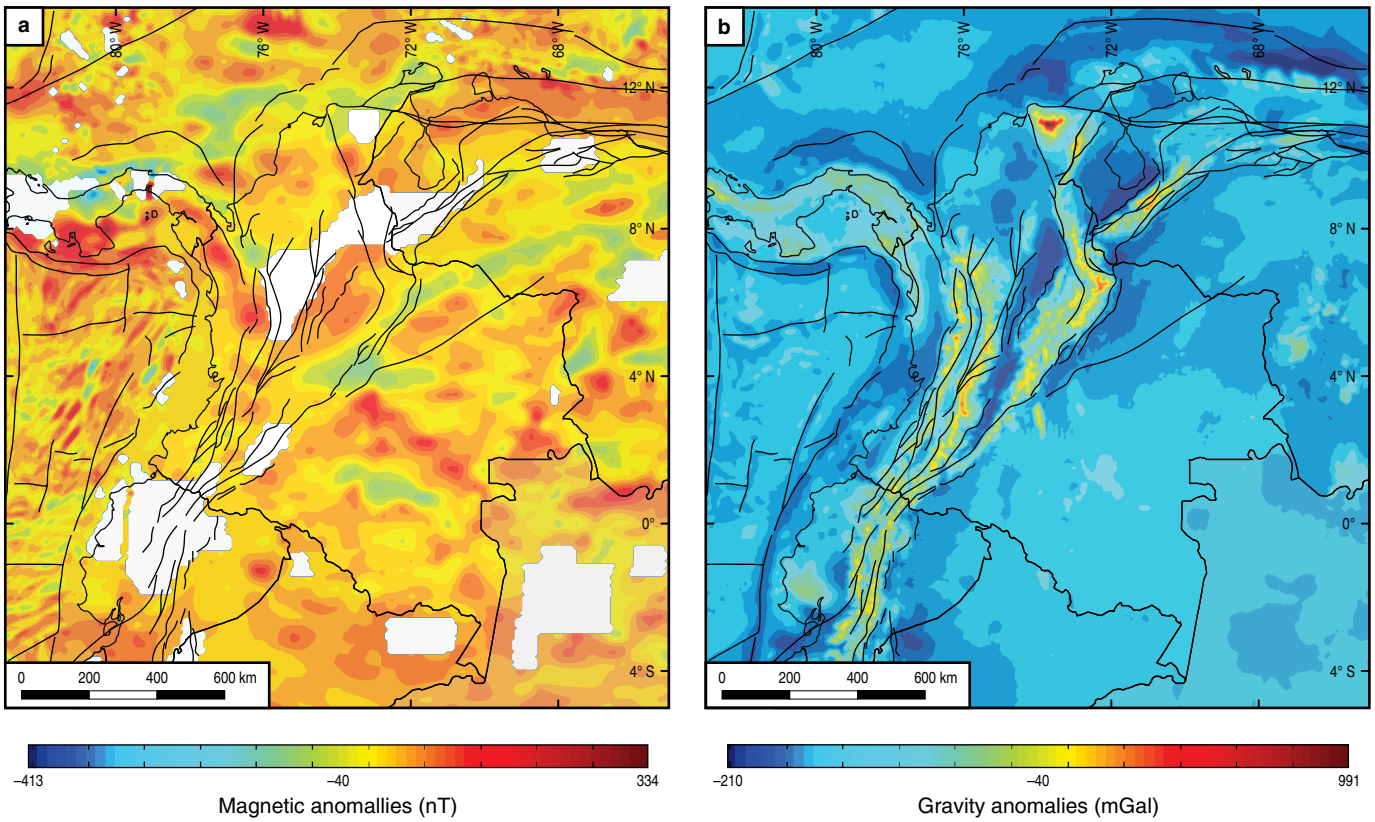

Figure 5. Observations of the potential field in the study zone used in this work. **(a)** Map of the total magnetic anomalies extracted from the World Digital Magnetic Anomaly Map–WDMAM version 2.0 (Dyment et al., 2015). **(b)** Free–air anomaly map obtained from the Earth Gravitational Model 2008–EGM2008 (Pavlis et al., 2012).

versions of the mesh oriented at different geographic trends (0°, 22°, 45°, and 67°). The results of these four inversions were then combined into a single model. Along each iteration within the LOTOS code, the workflow consisted of three main phases (Koulakov, 2009): (i) location of the events in the most up–to–date version of the model; (ii) calculation of the first derivative matrix; and (iii) inversion using the least squares algorithm.

3.5. Gravity Forward Modeling

Gravity forward modeling is typically used for testing hypotheses regarding the distribution of bodies and structures with contrasting densities. This work is used to confirm the geometry inferred based on previous techniques. The gravity dataset used in this article (Figure 5b) comes from the Earth Gravitational Model 2008–EGM2008 (see, e.g., Pavlis et al., 2012), which uses data from the Gravity Recovery and Climate Experiment (GRACE) satellite mission to establish a spherical harmonic model of the Earth's gravitational potential. Free–air anomalies were incorporated into the Oasis Montaj package version 9.1 to define a regular space grid and extract three profiles. These profiles were used to estimate forward models on the basis of density contrasts (Blakely, 1996), constrained by seismological estimates of the crust–mantle and the lithosphere–asthenosphere boundaries (Blanco et al., 2017; Poveda et al., 2015) to infer the subduction geometry in the most representative regions.

4. Results and Analysis

4.1. Regional Anomalies of Deformation

The distribution of the maximum and minimum directional axes of the horizontal projection of the strain ellipsoid (elongations *emax* and *emin*) is presented in Figure 6. Arrows suggest direction, and magnitudes of deformations are represented by the color scale. Contrasting domains west and east of the study area indicate a different response of the South American Plate during the converging process of the Nazca and Caribbean Plates. Though a lack of data in eastern continental regions and both ocean basins can promote interpolations that misrepresent the strain field, emax looks consistent with the presence of an indenter effect related to the Panamá Arc and surrounding areas. The extension of this effect may be somewhat bounded between the probable W–E lithospheric tear at approximately 5.5° N (called the Caldas Tear by Vargas & Mann, 2013) and the Santa Marta–Bucaramanga Fault System (SMBF; Figures 1, 2, 3). It is also notable that the SW anomaly could be induced by the Carnegie Ridge convergence under the South America Plate.

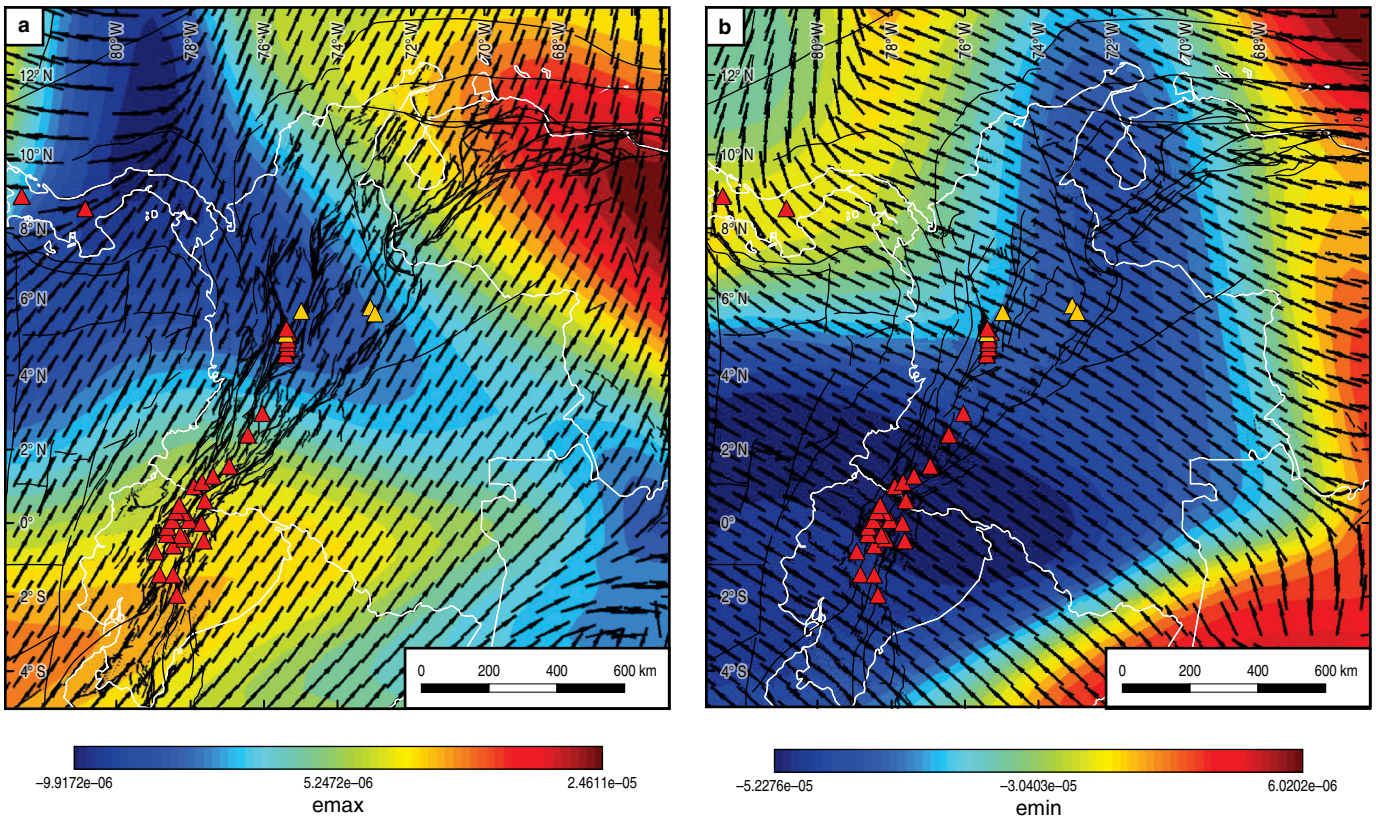

Figure 6. Maps of the strain field based on GPS observations. Estimations were performed with the SSPX program (Cardozo & Allmendinger, 2009). Calculations for **(a)** emax and **(b)** emin. Arrows show only the direction and colors the relative value of strain ellipse axes.

Large anomalies in emin in eastern Colombia may suggest a buttress effect that reduces the mobility of the western margin and promotes absorption of the stresses in the NW Andean Block. The direction of emax is consistent with the scape of the NW Andean Block, as suggested by Egbue & Kellogg (2010), but also with the mantle flow inferred by S–wave splitting (Idárraga–García et al., 2016), probably implying lithosphere–asthenosphere coupling in NW South America. The anomalies located in the NW part of the study region may indicate changes in the pattern of mobility of the western Caribbean Plate, possibly related to interactions with the North American Plate or local effects in the kinematics near the Hess Escarpment. The anomalies located in the SE that suggest a divergent pattern could be an artifact of the method or should be analyzed later in the light of other relevant information.

4.2. Mapping the Curie Point Depth

The Curie point depth (CPD) and its own uncertainty maps are presented in Figure 7. The maps show a SW–NE trend along the Andes range, highlighting a cold belt that interrupts the thermal field of NW South America. Although the CPD distribution corresponds to an overfiltered image, the cold belt looks divided near south of the Caldas Tear. The map also highlights the different values between continental areas and oceanic domains and shows how low CPD values are in the Panamá Basin in comparison to those in the Caribbean Basin. The mean values of CPD are located in the SE part of the study area (around the Amazon zones of Colombia, Venezuela, and Brasil) and in continental areas of NW Colombia and the Panamanian Isthmus. The SMM has deeper CPD values in contrast to the NW Colombia margin.

The errors associated with these estimations are located mainly in zones where the CPD is deeper, e.g., the southern zone. It is also notable that there are more significant errors near the borders between Colombia and Perú and between Colombia and Ecuador.

4.3. Vp, Vs, and Vp/Vs Ratio

A total of 113 269 local earthquakes associated with 849 830 picks (453 074 P picks and 396 756 S picks) were considered for estimating velocity anomaly tomograms (Figure 8). Damping values were selected based on synthetic tests with realistic data. Final variance reductions for P and S rays of 28.63% and 30.71%, respectively, were reached after the third iteration. Figures 9, 10 show examples at 10 and 130 km depth with the original checkerboard that incorporated velocity anomalies (upper panel). The middle panel presents the recovery of synthetic anomalies with the dataset with an acceptable solution, suggest-

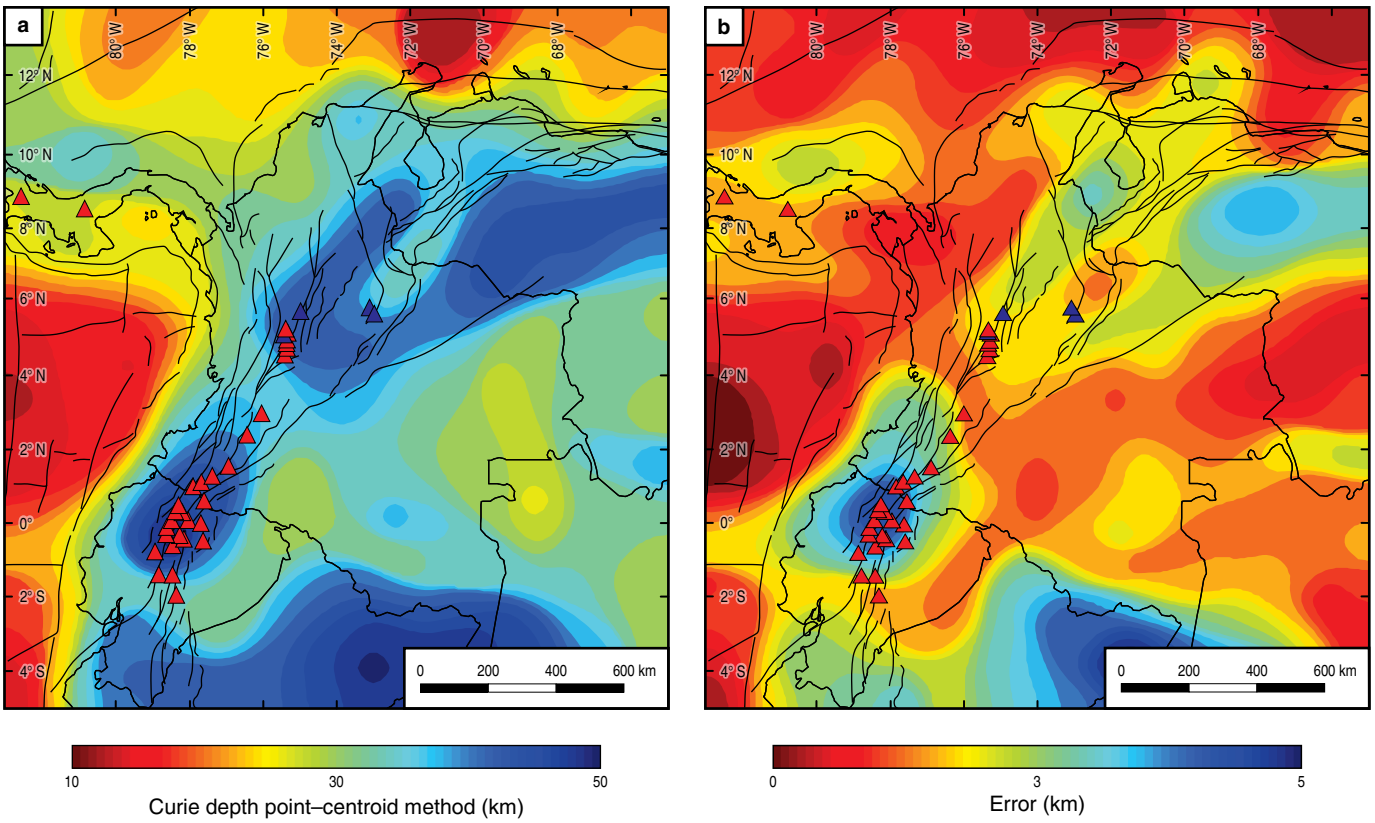

Figure 7. Estimations of the Curie point depth (CPD) using the centroid method (Okubo et al., 1985). **(a)** Map of CPD. **(b)** Map of errors.

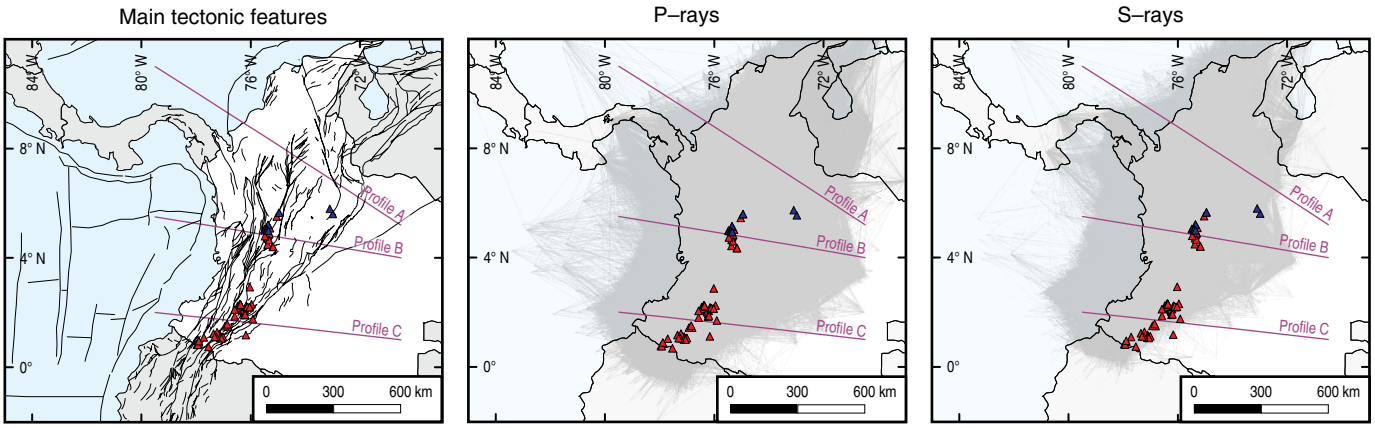

Figure 8. Coverage of P and S rays associated with 113 269 local earthquakes recorded by the RSNC. Purple lines correspond to vertical profiles presented in this work.

ing that the rays used may detect anomalies with horizontal dimensions of approximately 50 × 50 km. The lower panel shows the real inversion of Vp and Vs anomalies, as well as the Vp/Vs ratio. Along with several of the eight depth sections (10 km, 40 km, 70 km, 130 km, 180 km, 200 km, 250 km, and 300 km), velocity anomalies persist. For example, in this section at a depth of 130 km (lower panel), a low Vp anomaly aligns with the Santa Marta–Bucaramanga Fault System (see red arrow outside of the figure). Considering that at approximately this depth there are processes of slab mantle dehydration that promote buoyancy of new magma (see, e.g., Hasegawa & Nakajima, 2017; Paulatto et al., 2017), it seems consistent to relate the low–value anomalies in Vp and Vs to the presence of magmatic bodies near the Santa Marta–Bucaramanga Fault System (see Figures 1, 10).

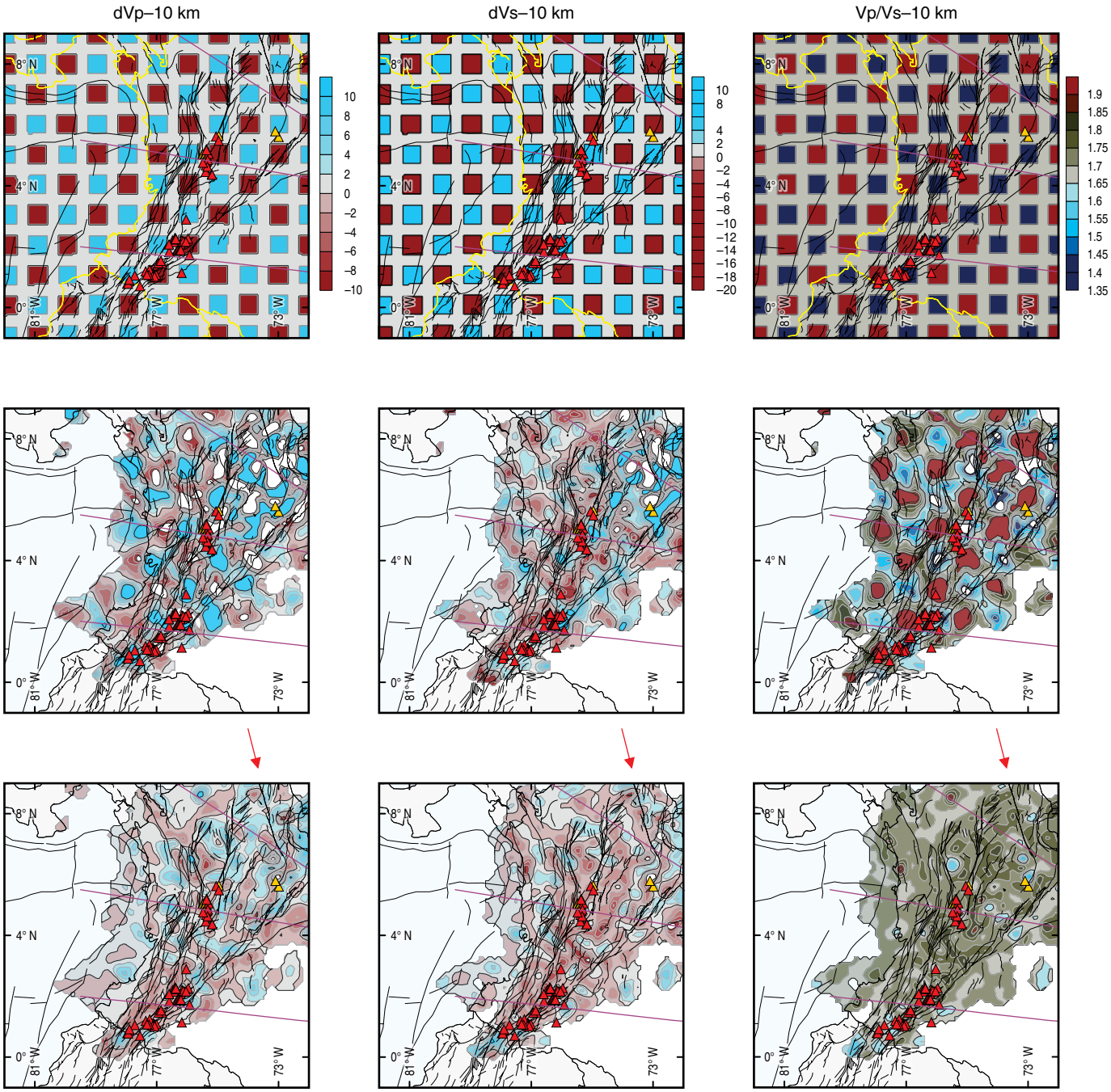

Figure 9. Synthetic velocity tomograms at 10 km. The upper panels show checkerboards with contrasting velocity anomalies that were reconstructed (middle panels) with the available dataset of first–arrival times of the P and S phases. Lower panels show the real tomograms. Red arrows suggest a different low–value anomaly in Vp aligned with the Santa Marta–Bucaramanga Fault System. This anomaly is present at depths ranging from 70 to 180 km.

Figure 11 shows synthetic tests and real estimates of Vp and Vs anomalies, as well as the Vp/Vs ratio, along the three profiles presented in this work. As each profile represents a corridor, it is possible to incorporate artifacts, distortions, or blurred regional structures as a consequence of averaging lateral velocity anomalies. However, Profile A shows Vp and Vs anomalies that may suggest the subduction process of the Caribbean Plate. The Vp/Vs ratio also highlights this structure. Profile B looks fuzzy, indicating that slab mantle dehydration and magmatic process are generating fluids and mineral phases that pervasively modify the structure of the Nazca Plate during the early stages of subduction. Profile C does not offer a clear image of the structure or process due to the short distance restored and the low resolution.

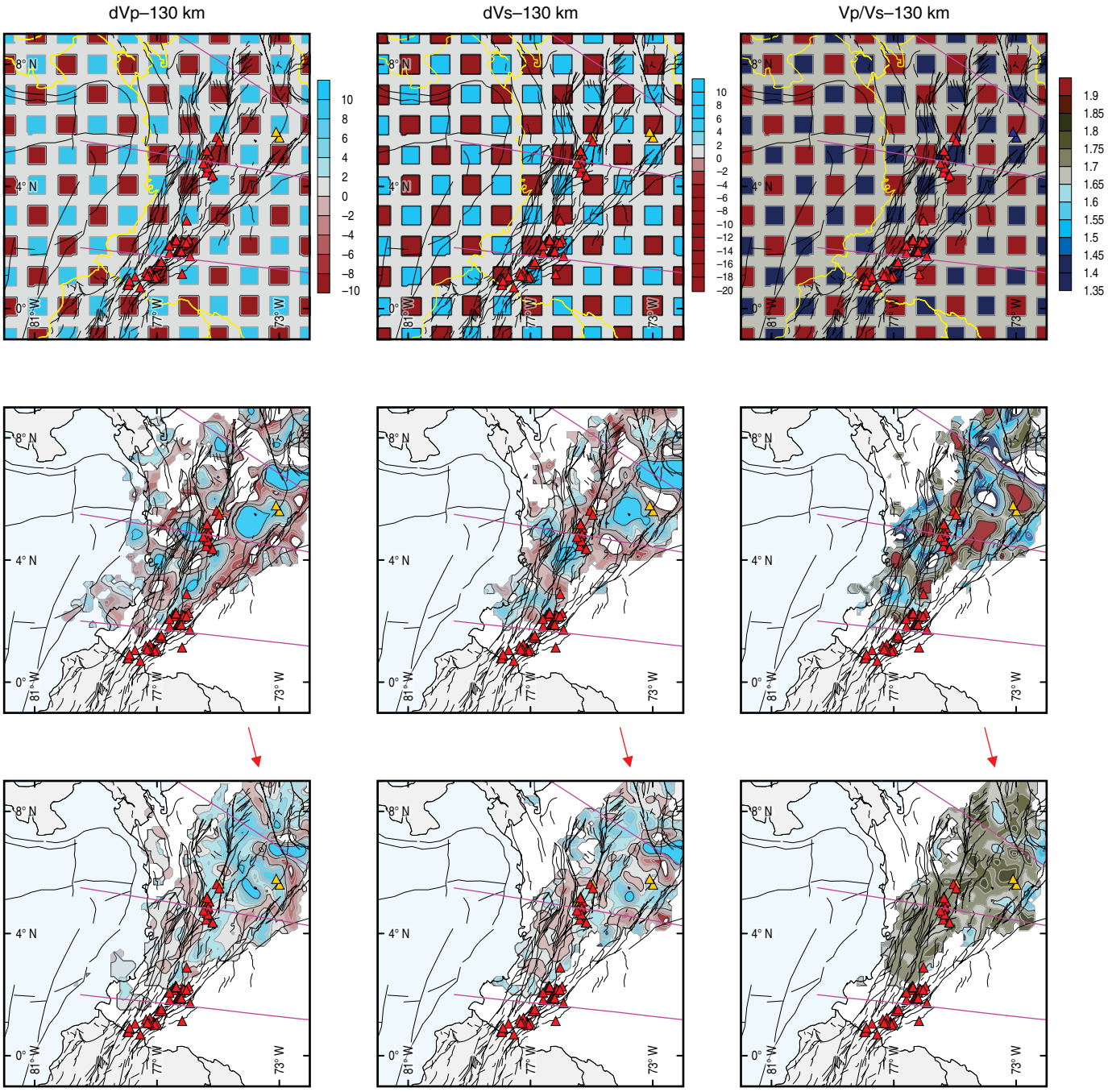

Figure 10. Synthetic velocity tomograms at 130 km depths. The upper panels show checkerboards with contrasting velocity anomalies that were reconstructed (middle panels) with the available dataset of first–arrival times of the P and S phases. Lower panels show the real tomograms. Red arrows suggest a different low–value anomaly in Vp aligned with the Santa Marta–Bucaramanga Fault System. This anomaly is present at depths ranging from 70 km to 180 km.

4.4. Representative Sections and Forward Gravity Modeling

Three representative sections located at different latitudes in NW South America (see Figure 1 for locations of the sections) present distinct responses associated with the subduction process. Figures 12, 13, 14 show the assemblage of topography, as well as observed and calculated gravity (upper panel) from forward modeling (middle panel) with the vertical representation of focal mechanisms and seismicity with the b–value distribution (lower panel).

Proposed models that satisfied the best fit of the gravity parameter have errors ranging between 49.0% and 61.6% (north: 51.6%; center: 61.6%; and south: 49.0%) due to some particular observed anomalies that are difficult to match. In general terms and for the sake of minimizing errors, the sections suggest a

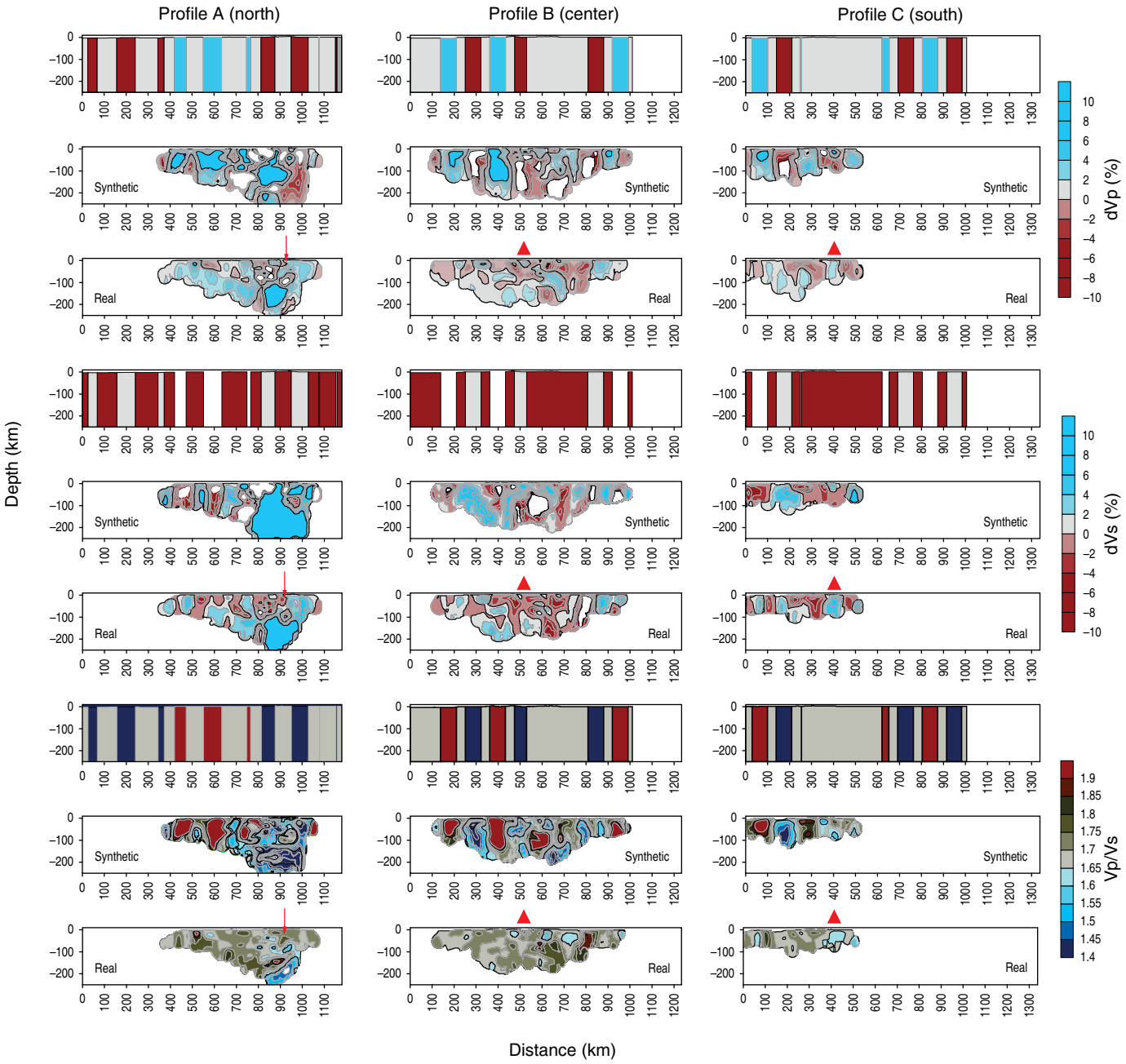

Figure 11. Profiles of velocity anomalies suggested in Figure 8. Upper panels are synthetic distributions derived from the checkerboards. Middle panels correspond to reconstructions of the synthetic checkerboards with the available dataset of first–arrival times of P and S phases. Lower panels show the real tomograms. Red arrows indicate the locations of the Santa Marta–Bucaramanga Fault System, and red triangles indicate the active volcanic arcs.

broad spectrum of densities that must be incorporated in the continental lithosphere around zones of the plate that start to sink. In these zones, the CPD trends tend to be unstable as a consequence of the interaction between different thermal regimes and the influx of water and sediments into the subduction channel. Consequently, a broad range of depth–magnitude seismicity is observed that promotes zones of different b–values, most likely associated with abrupt variations in the pressure–temperature field accompanied by mineral transformations during the subduction process.

5. Discussion

Estimates presented in this work suggest at least eight key aspects that evidence the complexity of the subduction process in NW South America: (i) segmentation of the Wadati–Benioff

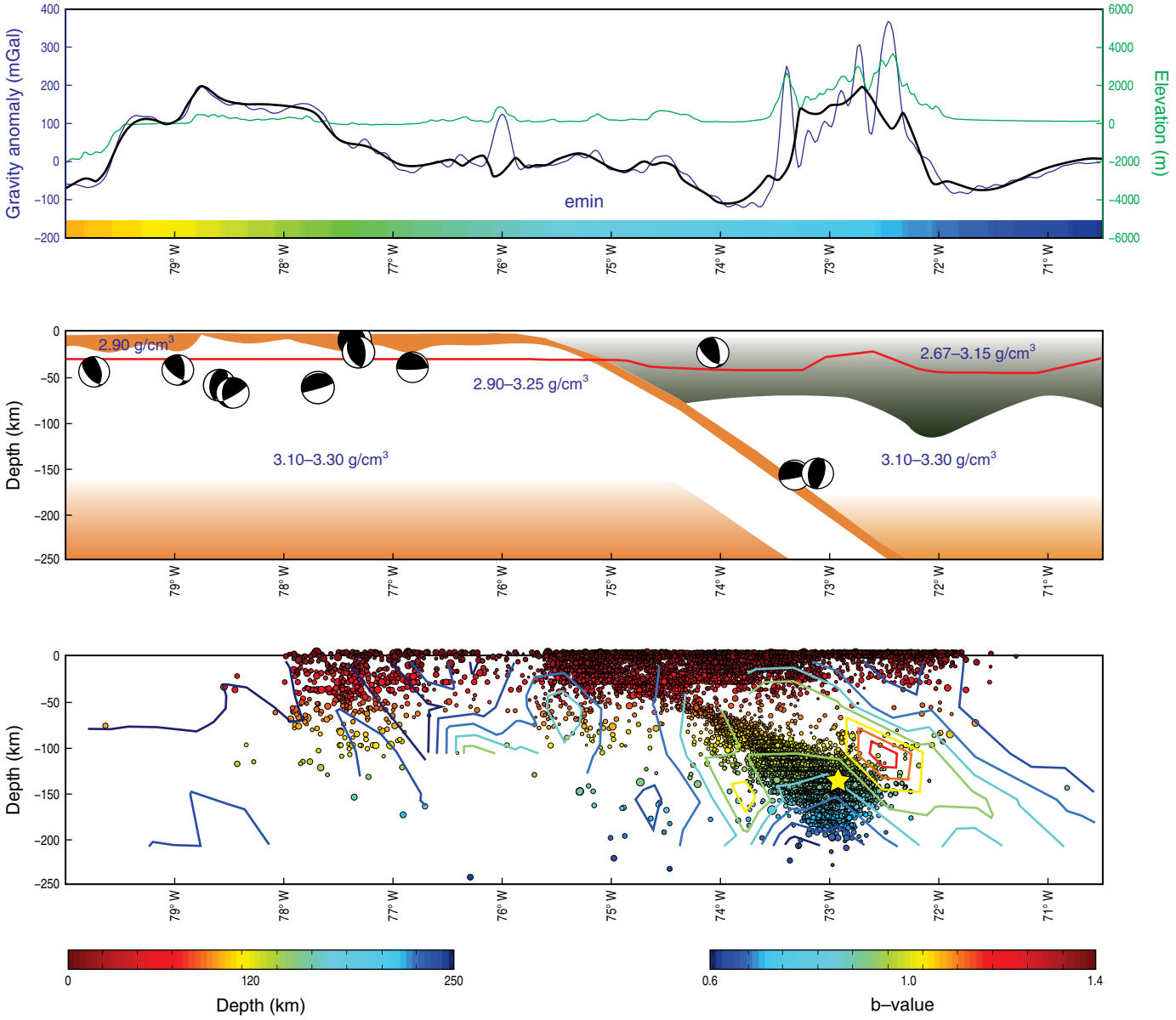

Figure 12. Profile A in the north is indicated in Figure 1. The upper panel represents the free–air anomaly observed (blue line) and calculated (black line). Exaggerated topography is represented with green lines. The colored band located in lower part of this panel represents the variation of the emin along the profile (see Figure 6). Middle panel shows the proposed model of subduction based on density variations and thickness of the crust and the lithosphere–asthenosphere boundaries reported by Poveda et al. (2015) and Blanco et al. (2017). Focal mechanisms are vertical projections on the section. Lower panel shows seismicity in a corridor 50 km wide and the iso–lines of b–values. The red line in the middle panel corresponds to the Curie point depth isotherm. Yellow star in the lower panel shows the approximate location of the Bucaramanga nest.

topography (Figure 15), following the axis trend of the Sandra Ridge–Caldas Tear (see Figures 1, 3, 15, approximately 5.5° N); (ii) an indenter effect related to the Panamá Arc highlighted by the strain field pattern (see, e.g., emin in Figure 6) and bounded by the same axis trend; (iii) angular variation in the subduction geometry (see Figures 12, 13, 14), changing from low angles in the north (ca. 12 to 24°) to steeper in the central region (ca. 34°) and less steep in the southern areas (ca. 30°); (iv) the presence of a volcanic arc that is distributed along three thermal zones to the south of the Caldas Tear (Figure 7) and no presence of active magmatism to the north of this structure; (v) the distinct thermal responses of the Nazca and Caribbean Plates associated with differential expression of the bathymetric relief (Figures 1, 7); (vi) the presence of low–value anomalies in Vp and Vs along the volcanic arc and the Santa Marta–Bucaramanga Fault System; (vii) the near–extinction of seismicity inside or below the Antioquian Batholith and south of the Eastern Cordillera (Figure 3); and (viii) shallowing of the seismicity in the NW corner of the Santa Marta Massif (Figure 15). Based on these aspects, there is substantial evidence that may contribute to an-

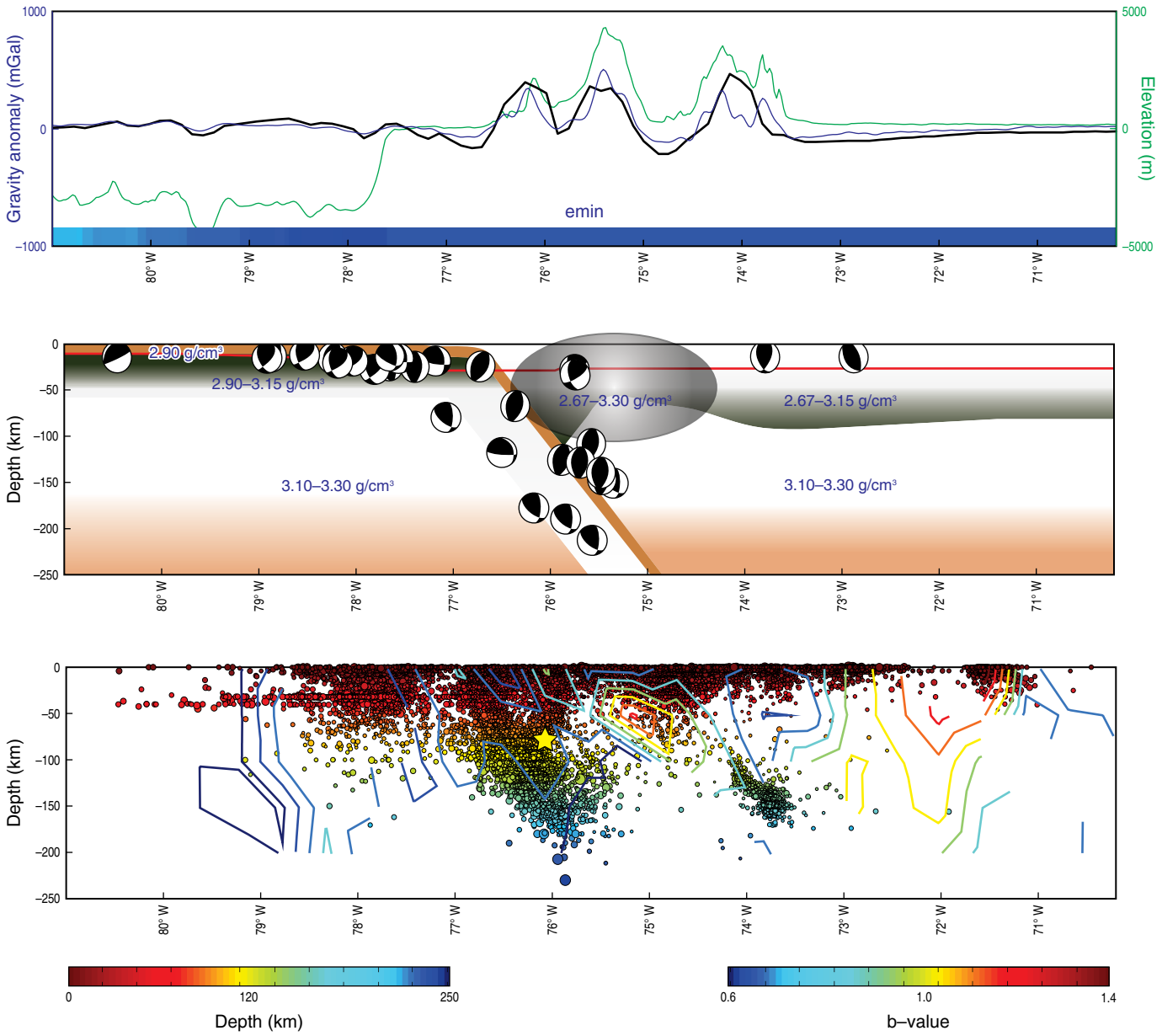

Figure 13. Profile B in the central region is indicated in Figure 1. The upper panel represents the free–air anomaly observed (blue line) and calculated (black line). Exaggerated topography is represented with green lines. The colored band located in lower part of this panel represents the variation of the emin along the profile (see Figure 6). Middle panel shows the proposed model of subduction based on density variations and thickness of the crust and the lithosphere–asthenosphere boundaries reported by Poveda et al. (2015) and Blanco et al. (2017). Ellipse indicates the zone of complex and contrasting densities. Focal mechanisms are vertical projections on the section. Lower panel shows seismicity in a corridor 50 km wide and the iso–lines of b–values. The red line in the middle panel corresponds to the Curie point depth isotherm. Yellow star in the lower panel shows the approximate location of the Cauca nest.

swering some fundamental questions about the seismotectonics and the subduction process in this region.

5.1. Why Is the Wadati–Benioff Zone Displaced towards the East? Why Is the Volcanic Arc Segmented?

Vargas & Mann (2013) proposed that since 9–12 Ma, the Panamá Arc, coupled with the older plateau that constitutes the Caribbean Plate (Kerr & Tarney, 2005), acts as a tectonic indenter in NW South America, promoting an eastward seismic offset (ca. 240 km long) called the Caldas Tear, which is collinear with the Sandra Rift. The lithospheric Caldas Tear controls the distribution of seismicity and consequently promotes the offset of the Wadati–Benioff topography (Figure 15). The weakness zone that comprises the Caldas Tear and the Sandra Rift represents a solution to the regional normalization analysis proposed by Keppie (2014), which based on geometric approaches

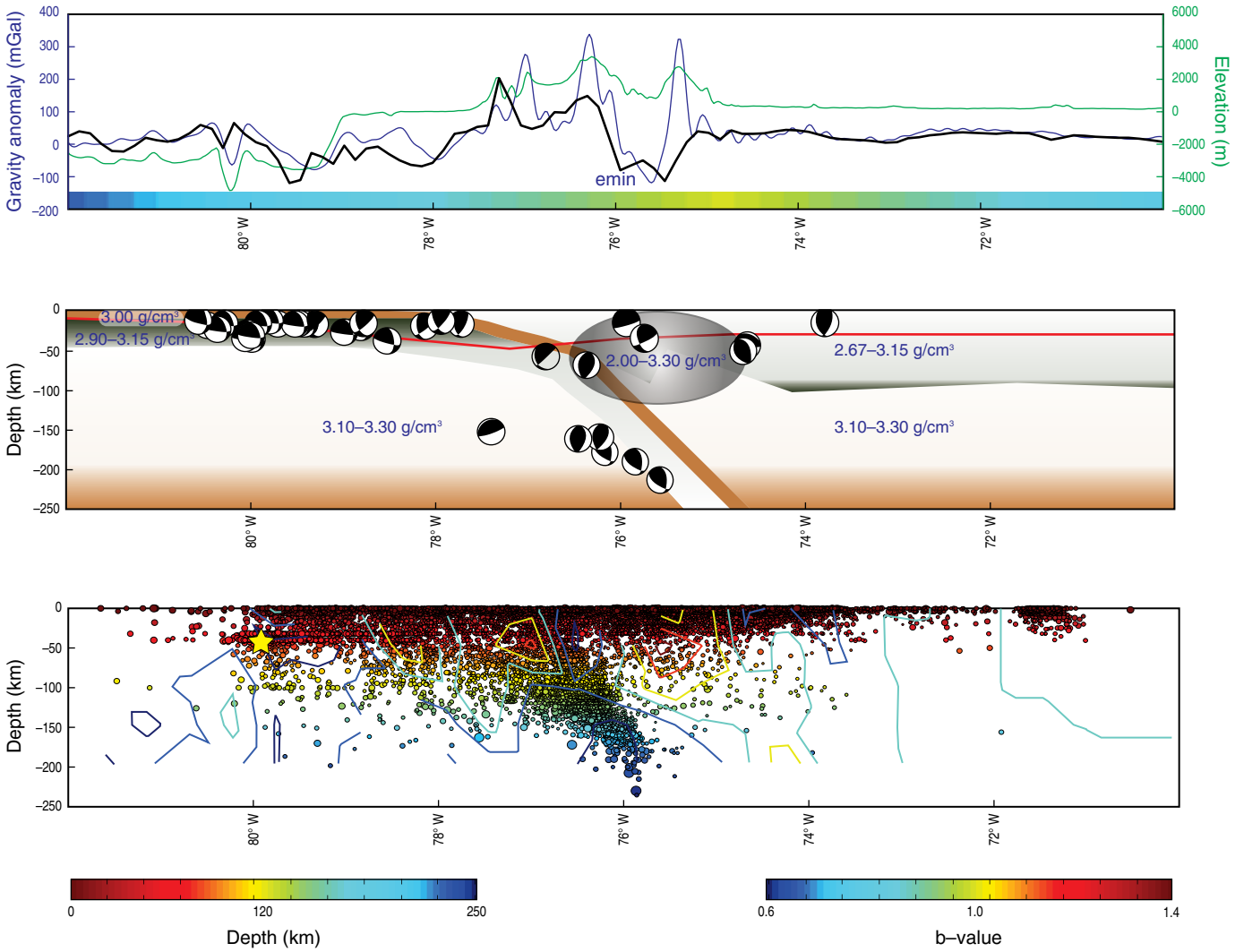

Figure 14. Profile C in the south is indicated in Figure 1. The upper panel represents the free–air anomaly observed (blue line) and calculated (black line). Exaggerated topography is represented with green lines. The colored band located in lower part of this panel represents the variation of the emin along the profile (see Figure 6). Middle panel shows the proposed model of subduction based on density variations and thickness of the crust and the lithosphere–asthenosphere boundaries reported by Poveda et al. (2015) and Blanco et al. (2017). Ellipse indicates the zone of complex and contrasting densities. Focal mechanisms are vertical projections on the section. Lower panel shows seismicity in a corridor 50 km wide and the iso–lines of b–values. The red line in the middle panel corresponds to the Curie point depth isotherm. Yellow star in the lower panel shows the approximate location of the Tumaco mega–earthquake zone.

and hypothetical triple junctions, suggests that this zone represents the southern border of the Caribbean Plate (Figure 16a). In this sense, Salazar & Vargas (2015), using seismotectonic deformation derived from focal mechanisms and GPS vectors, also related this weakness zone to the southern border of the Caribbean Plate (Figure 16b).

If contrasting buoyancies of the Caribbean and Nazca Plates due to age, thickness, and thermal structure promote distinct subduction angles, it looks reasonable that the Caldas Tear becomes the current border between the two plates, and different magmatic responses should be expected. In addition, the tectonic indenter associated with the Panamá Arc may promote drag effects that propagate other shorter offsets with/without lithospheric tears and implications for the control of mantle flow (Figure 16, and see also, e.g., the Malpelo Tear proposed by Idárraga–García et al., 2016). Thus, segmentation of the lithosphere due to possible indenters may be responsible for the segmented volcanic arc, at least to the south of the Caldas Tear. Figure 17 presents a conceptual model that draws the subduction surface derived from the seismic surface, where in addition to the presence of possible tears, there is a dramatic change in the strike of the subduction surface in northern Colombia and Venezuela. In this figure is also suggested a possible transition zone between Nazca and Caribbean Plates supported in the earthquake distribution pattern at the north of the Caldas Tear.

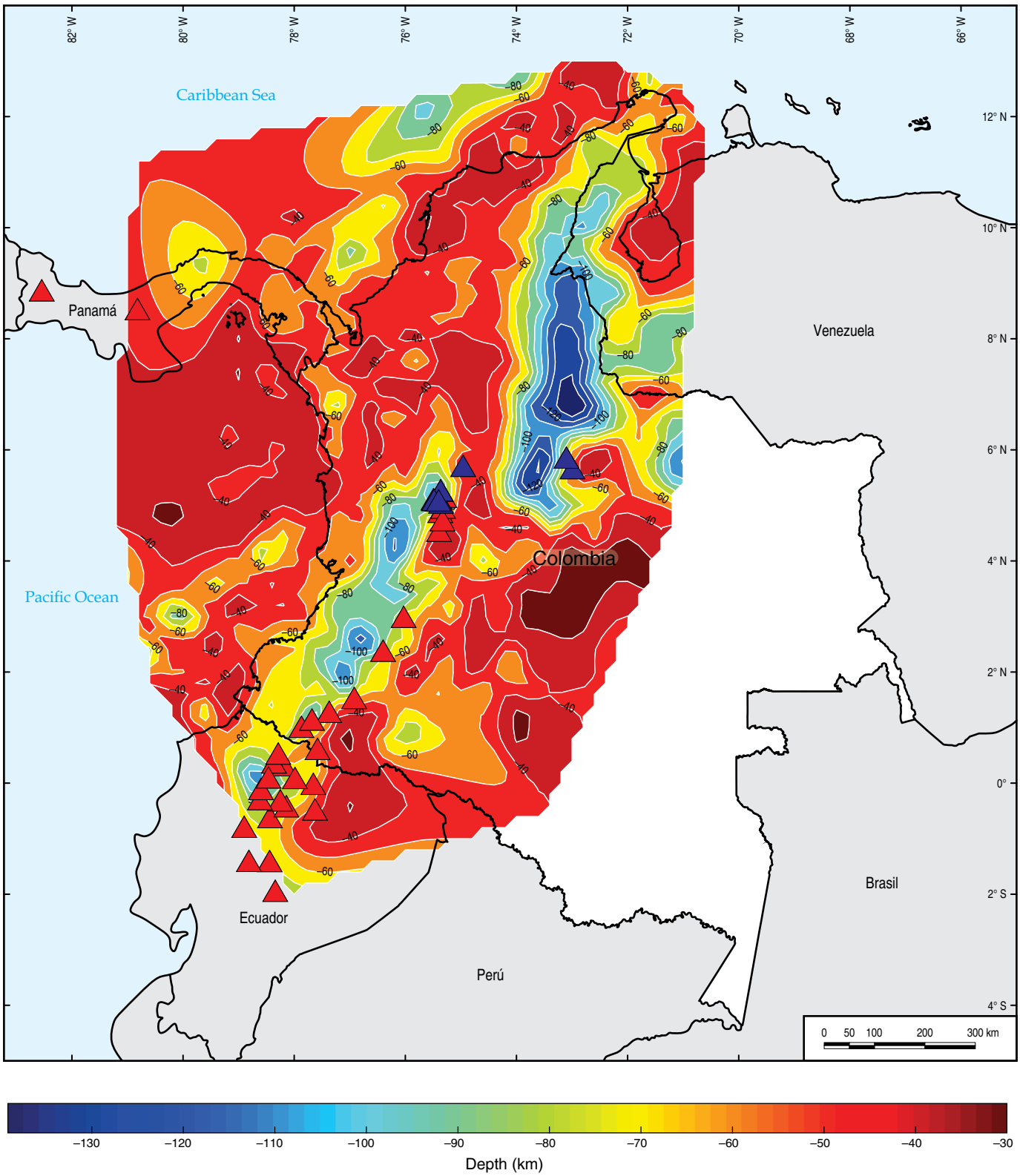

Figure 15. The seismic surface that best fits the most frequent and deeper events. The surface derives from averaging all events deeper than 20 km around areas of 50 × 50 km along the study area. This surface may highlight the brittle–ductile transition zone and the Wadati–Benioff surface.

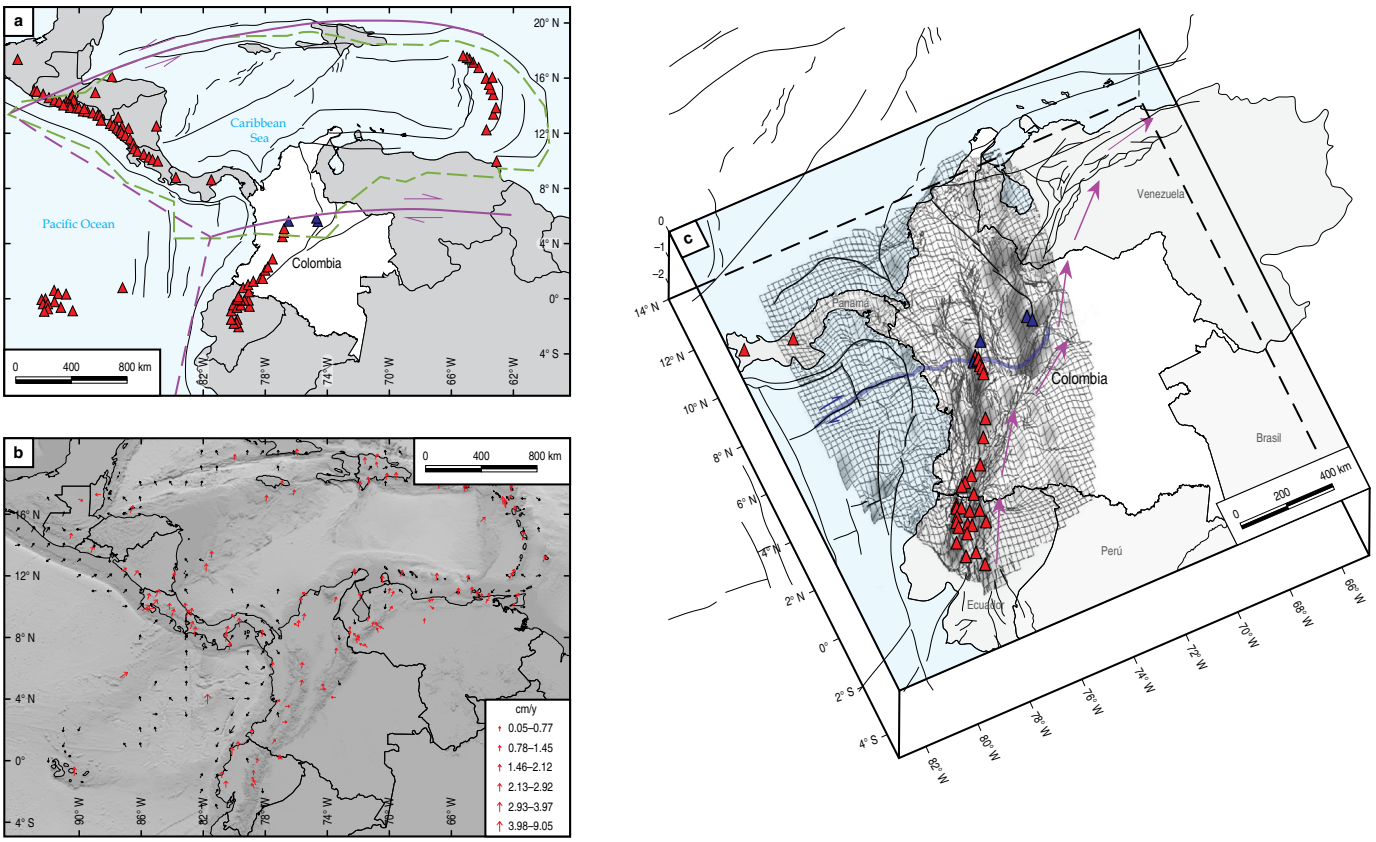

Figure 16. (a) Kinematic boundary solution for the Caribbean Plate based on geometric approaches and hypothetical triple junctions (purple lines) and suggested by Keppie (2014). **(b)** A similar solution for the southern boundary of the Caribbean Plate proposed by Salazar & Vargas (2015) interpreting seismotectonic deformation derived from GPS observations (red arrows) and focal mechanisms (black arrows). **(c)** Seismic surface with the collinearity of the Sandra Ridge and Caldas Tear (blue line), suggesting the southern boundary of the Caribbean Plate. Volcanoes are indicated with triangles (active: red; inactive: blue). The mantle flow estimated by S–wave splitting (Idárraga–García et al., 2016) is represented by purple arrows.

5.2. What Explains the Presence of Several Seismic Nests in NW South America?

The nature of this phenomenon is complicated to describe, despite the efforts made over the last three decades and from different strategies (see, e.g., Schneider et al., 1987; van der Hilst & Mann, 1994; Frohlich et al., 1995; Taboada et al., 2000; Cortés & Angelier, 2005; Frohlich, 2006; Zarifi, 2006; Prieto et al., 2012, 2013; Vargas & Mann, 2013). Neither lateral variations in velocity anomalies nor the Vp/Vs ratios estimated in this work represent robust evidence about conditions or processes related to the seismic nests in this region. However, a projection of the CPD estimates on the seismic surface suggests contrasting thermal anomalies around the Bucaramanga and Cauca nests (see Figures 7, 18). Thus, although it is not possible to discard mechanisms related to propagation of break–off due to collision of structures, gravitational collapse of the subducted slabs by densification, and simple shear runaway, it is possible to explain this anomalous seismicity with thermal instabilities related to shear runaway (see, e.g., Poli et al., 2016) and weakness by intense dehydration processes, particularly for the Bucaramanga nest.

On the other hand, Syracuse et al. (2016) report a fault oriented approximately N65°E and extending from the western coast of Colombia near 6° N through the Western and Central Cordilleras. Per this author, seismicity associated with the reported structure extends through the entire crust, from the surface to 50–60 km depth, with approximately 60% of the seismicity in the upper 20 km of the crust. A careful inspection of this pattern allows us to distinguish at least three small clusters related to regional faults that trend almost NNW (Murindó, Murrí, and/or Mutatá Faults, see, e.g., Mosquera–Machado et al., 2009), which, due to density of information and scale of visualization, give the impression of a fault with tendency almost ENE (Figure 3). Hence, for the Murindó nest, an ENE regional fault is discarded, as has been proposed.

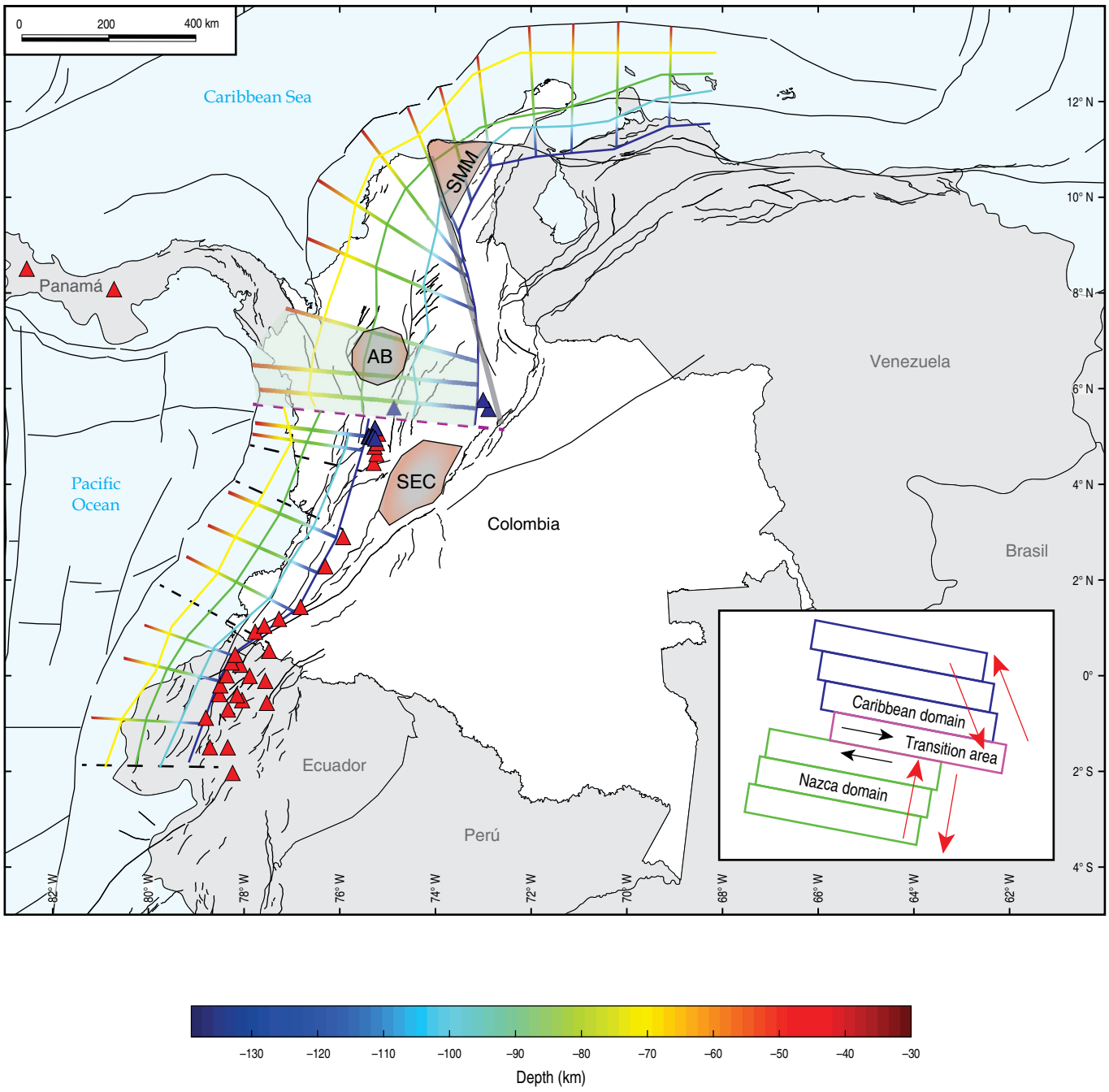

Figure 17. Wire model based on the seismic surface. The Caldas Tear is highlighted by the purple dashed line. Other tears in the Nazca Plate are suggested with black dashed lines. Another probable tear zone is aligned with the surficial projection of the Santa Marta–Bucaramanga Fault System (SMBF, gray and degraded line). Although it is possible a flat subduction along NW Venezuela, in this figure is presented as an alternative hypothesis a steeper subduction, which mechanically is coherent with the structural features observed in this region. The Santa Marta Massif (SMM) is being tilted southeastward as a mechanical response to the changes in dip and strike of the Caribbean Plate, which implies an exhumation rate higher in the NW corner of the Santa Marta Massif than in the south end of the Santa Marta–Bucaramanga Fault System. The Antioquian Batholith (AB) and the southern region of the Eastern Cordillera (SEC, composed of the metamorphic belt of the Garzón and Quetame Massifs) are coherent and rigid blocks that transfer strain from the west to the east boundaries without internal fracturing and are involved in the crust during the subduction process. The lack of seismicity within these blocks suggests that still varying compositional and elastic properties at depth, they maintain coherence as structural blocks beyond the upper crust. Transparent polygon represents the possible transition area between Nazca to Caribbean Plates. The lower right inset shows schematic blocks that represent the effect of the Panamá tectonic indenter against NW South America, including the transition zone between Nazca and Caribbean Plates.

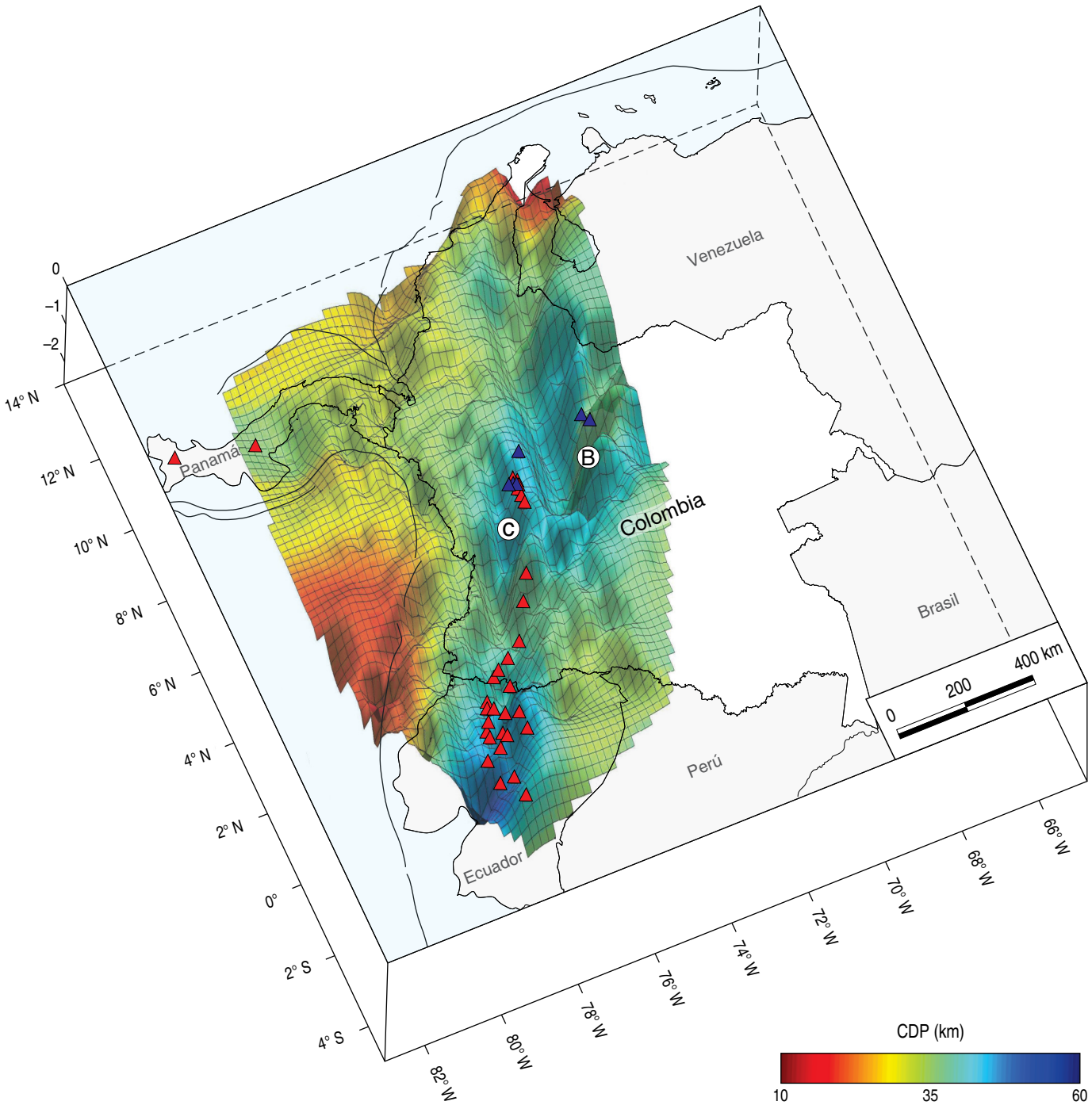

Figure 18. Three–dimensional representation of the seismic surface coupled with the projection of the Curie depth point estimations. The Bucaramanga (B) and Cauca (C) nests are located near thermal anomalies.

5.3. What Controls the Scarce Seismicity in the Continental Areas of the Sinú–San Jacinto and Lower Magdalena Basins, Panamá, and the Santa Marta Massif?

Seismicity in this region is scarce but not absent, suggesting low activity that increases eastward and deeper. An interpretation of this pattern is related to the change in the subduction angle of the Caribbean Plate under the South American Plate, passing from approximately 12° to >24° under the Middle Magdalena Valley Basin. As seismic absorption becomes higher to the east (Eastern Cordillera and serranía de Perijá), an abrupt change in the subduction angle promotes strain absorption at depth that is manifested by seismicity. These observations have been suggested in the wire model (Figure 17), where the

steepest subduction angle is near the Santa Marta Massif, north Colombia, and Venezuela. Mazuera–Rico (2018) using a new active seismic experiment (GIAME), as well interpretations derived from previous works using receptor functions (Masy et al., 2015; Quinteros, 2007), and gravity modeling (Blanco et al., 2015), has suggested flat subduction of the Caribbean Plate under NW Venezuela. Although it is possible this hypothesis, resolution of the receptor function analyses does not allow to appreciate this process clearly. Alternatively, a steeper subduction (Pérez & Mendoza, 1998) may be a converging solution that mechanically produce same structural features observed in this region and can be also modeled with gravity datasets. Last solution also agrees with the present–day dextral wrench system in northern Colombia and Venezuela, which is composed of the Oca–San Sebastián–El Pilar–Los Bajos–El Soldado System (Ramos, 2015).

On the other hand, it is widely accepted that the Caribbean Plate has been subducting under northern South America for 75 Ma with very little magmatic activity, probably because it is buoyant and subduction is slow with a shallow dip. However, the results presented in this work suggest that the negative velocity anomaly observed in the tomogram at a depth of 130 km (Figure 10) and the probable mechanical response of a segment of slab that changes strike drastically are producing a weakness zone (tear?), where material derived from dehydration tries to ascend but is accommodated along this corridor. Attending this assumption, the projection of the entire Santa Marta–Bucaramanga Fault System corresponds to a weakness zone created by emplacement of magmatic material, which does not promote enough pathways for quick ascent and production of a volcanic arc due to the convergence regime. However, it is possible that during the last 9–12 Ma, under the critical influence of the Panamá Arc against NW South America, other emplacements of magmatic material took place along this orogenic system (see, e.g., Mantilla–Figueroa et al., 2011). Mechanically, this hypothesis matches surficial observations. Thus, a local change in the subduction direction of the Caribbean Plate or the subduction of a bathymetric relief (Waller II & Frost, 2018) may imply an exhumation rate higher in the NW corner of the Santa Marta Massif than in the south end of the Santa Marta–Bucaramanga Fault System. In this sense, Villagómez et al. (2011) suggest that although exhumation is not recorded after ca. 16 Ma, the high elevation and high erosive power of the climate in and around the Santa Marta Massif imply that the rock and surface uplift that gave rise to the current topography is very recent (i.e., ≤1 Ma?), with insufficient time to expose the fossil apatite partial annealing zone. Similarly, although with the same limitations of resolution as apatite and zircon fission tracks, Amaya et al. (2017) present observations of exhumation at the south end of the Santa Marta–Bucaramanga Fault System in the Santander Massif but with lower intensity than in the Santa Marta Massif.

5.4. What Governs the Segmented Seismicity along the Colombia–Ecuador Trench? How Can the Contrasting Pattern of Focal Mechanisms along This Region Be Explained?

Bathymetric relief and large gravity anomalies in the Pacific Ocean and the western margin of NW South America suggest the presence of oceanic ridges that are being incorporated into the subduction process, generating high seismic activity with gaps probably related to stagnation of promontories that accumulate elastic energy. This interpretation is consistent with the distribution of b–values observed in this work.

At least two zones present domains of focal mechanisms. South of 2° N, the trench seismicity suggests a consistent process of normal faults due to the bending of the Nazca Plate in areas proximal to the trench. North of this latitude, there is a mixture of focal mechanisms varying from pure normal to strike–slip faults. This different pattern reveals the role that more homogeneous bathymetric relief at the south plays, probably influenced by the Carnegie Ridge, and the contrasting area is more affected by small ridges and rifts that are being subducted.

5.5. Why Is Seismicity Scarce inside the Antioquian Batholith and South of the Eastern Cordillera?

The Antioquian Batholith corresponds to four granitoid bodies of Late Cretaceous age (Ibañez–Mejia et al., 2007; Ordóñez–Carmona et al., 2001), most likely connected compositionally to other batholiths of the Central Cordillera. Restrepo–Moreno et al. (2009) suggested at least two pulses for its exhumation that coincide with orogenic phases observed in the Colombian, Peruvian, Bolivian, and Argentinean Andes and some orogenic systems of the Caribbean region. These authors proposed that the whole body was uplifted and exhumed as a coherent structural block, corroborating other structural evidence for the rigidity and coherence of this crustal block in the northern Andes.

The Antioquian Batholith has scarce interior seismicity, although superficial activity surrounds it. Three small earthquake swarms that constitute the Murindó nest (north) seem to be part of this aureole of seismicity (Figure 3). The eastern shallow seismicity of the Middle Magdalena Valley is related to the Caribbean slab, which starts a steeper angle of subduction. The geometry of the batholith and its seismicity pattern may be interpreted as reflecting a coherent structural block (in the sense of Restrepo–Moreno et al., 2009), in which rigidity may transfer strain from west to east in the block and which was involved in the crust during the pushing process of the Panamá indenter on NW South America during the last 9–12 Ma (Vargas & Mann, 2013). In addition, the lack of seismicity at depth is

the response of a body that still, with varying compositional and elastic properties at depth, maintains coherence as a structural block beyond the upper crust.

At the south of the Bogotá Savanna, in the Eastern Cordillera, another zone with a lack of seismic activity appears (Figure 3). Eastward of this region, there is again superficial activity associated with the foothill fault system (Frontal Llanos Fault System), and westward seismic events related to superficial faults and the subduction process of the Nazca Plate appear. The zone is dominated by old metamorphic rocks (granulites, gneisses, amphibolites, and minor ultramafic and calc–silicate rocks that constitute mainly the Garzón and Quetame Massifs) with ages ranging from Mesoproterozoic to Cambrian (see, e.g., Saeid et al., 2017). As in the case of the Antioquian Batholith, the rigidity of this block may transfer the strain derived from the subduction process from west to east, generating high seismic activity along its borders and suggesting that compositional and elastic properties at depth maintain its coherence as a structural body beyond the upper crust of the South America Plate.

6. Conclusions

Seismological, geodetic, gravity, and magnetic public datasets were used to investigate the subduction process in NW South America. Estimates of three–dimensional velocity tomography, Curie depth points, and the strain field in the upper crust show complex interactions among the Caribbean, Nazca, and South America Plates.

A wire model supported by three profiles is proposed for explaining the subduction process and the interaction of the lithospheric plates, highlighting a broad range of subduction styles. In this model, several tear faults play relevant roles in mechanically accommodating changes in the dip and strike of the Caribbean and Nazca Plates under NW South America. Given these assumptions, it is proposed a flat subduction of the Caribbean Plate along NW South America, or alternatively may change from flat subduction in the south (near the Caldas Tear) to steeper subduction in the north, differentially uplifting the Santa Marta Massif and the Santander Massif along the Santa Marta–Bucaramanga Fault System. The model also hypothesizes that the absence of a modern volcanic arc in the Eastern Cordillera and/or the serranía de Perijá is a consequence of the compressional regime induced by the Panamá tectonic indenter, generating a zone of fluid accumulation at depth derived from the dehydration process; these fluids cannot ascend to surface, which impedes the formation of active magmatism. The wire model also shows that the low seismic activity within the Antioquian Batholith is a consequence of its rigidity, promoting the transfer of strain derived from the subduction process from west to east, generating high seismic activity along its borders and suggesting that compositional and elastic properties at depth maintain its coherence as a structural body beyond the upper crust. A similar interpretation is proposed for the southern part of the Eastern Cordillera, including the belt formed by the Garzón and Quetame Massifs.

Acknowledgments

Thanks to the Departamento de Geociencias of the Universidad Nacional de Colombia for partially supporting this research. Special gratitude to the Servicio Geológico Colombiano for sharing seismological information. Appreciation to COLCIENCIAS for partial funding through grant #FP44842–006–2016 "Análisis 4D de Vp, Vs y la relación Vp/Vs en la esquina NW de Suramérica". Sincere thanks to the reviewers Victor RAMOS (Universidad de Buenos Aires) and James KELLOGG (University of South Carolina), who gave constructive feedback for the improvement of the paper. I also appreciate the constructive support of the editorial team, especially that of the editor–in–chief, Jorge GÓMEZ TAPIAS.

References

Amaya, S., Zuluaga, C. & Bernet, M. 2017. New fission–track age constraints on the exhumation of the central Santander Massif: Implications for the tectonic evolution of the northern Andes, Colombia. Lithos, 282–283: 388–402. https://doi.org/10.1016/j.lithos.2017.03.019

Anderson, V.J., Horton, B.K., Saylor, J.E., Mora, A., Tesón, E., Breecker, D.O. & Ketcham, R.A. 2016. Andean topographic growth and basement uplift in southern Colombia: Implications for the evolution of the Magdalena, Orinoco, and Amazon river systems. Geosphere, 12(4): 1235–1256. https://doi.org/10.1130/GES01294.1

Bernal–Olaya, R., Mann, P. & Vargas, C.A. 2015. Earthquake, tomographic, seismic reflection, and gravity evidence for a shallowly dipping subduction zone beneath the Caribbean margin of northwestern Colombia. In: Bartolini, C. & Mann, P. (editors), Petroleum geology and potential of the Colombian Caribbean margin. American Association of Petroleum Geologists, Memoir 108, p. 247–269. https://doi.org/10.1306/13531939M1083642

Blakely, R.J. 1996. Potential theory in gravity and magnetic applications. Cambridge University Press, 441 p. California, USA. https://doi.org/10.1017/CBO9780511549816

Blanco, J.F., Vargas, C.A. & Monsalve, G. 2017. Lithospheric thickness estimation beneath northwestern South America from an S–wave receiver function analysis. Geochemistry, Geophysics, Geosystems, 18(4): 1376–1387. https://doi.org/10.1002/2016GC006785

Blanco, J.M., Mann, P. & Nguyen, L.C. 2015. Location of the Suture Zone separating the Great Arc of the Caribbean from continental crust of northwestern South America inferred from regional gravity and magnetic data. In: Bartolini, C.

& Mann, P. (editors), Petroleum geology and potential of the Colombian Caribbean Margin. American Association of Petroleum Geologists, Memoir 108, p. 161–178. https://doi.org/10.1306/13531935M1083641

Cardozo, N. & Allmendinger, R.W. 2009. SSPX: A program to compute strain from displacement/velocity data. Computers & Geosciences, 35(6): 1343–1357. https://doi.org/10.1016/j.cageo.2008.05.008

Carrillo, E., Mora, A., Ketcham, R.A., Amorocho, R., Parra, M., Costantino, D., Robles, W., Avellaneda, W., Carvajal, J.S., Corcione, M.F., Bello, W., Figueroa, J.D., Gómez, J.F., González, J.L., Quandt, D., Reyes, M., Rangel, A.M., Román, I., Pelayo, Y. & Porras, J. 2016. Movement vectors and deformation mechanisms in kinematic restorations: A case study from the Colombian Eastern Cordillera. Interpretation, 4(1): T31–T48. https://doi.org/10.1190/INT-2015-0049.1

Cediel, F., Shaw, R.P. & Cáceres, C. 2003. Tectonic assembly of the northern Andean Block. In: Bartolini, C., Buffler, R.T. & Blickwede, J. (editors), The circum–Gulf of Mexico and the Caribbean: Hydrocarbon habitats, basin formation, and plate tectonics. American Association of Petroleum Geologists, Memoir 79, p. 815–848. Tulsa, USA.

Chiarabba, C., De Gori, P., Faccenna, C., Speranza, F., Seccia, D., Dionicio, V. & Prieto, G.A. 2016. Subduction system and flat slab beneath the Eastern Cordillera of Colombia. Geochemistry, Geophysics, Geosystems, 17(1): 16–27. https://doi.org/10.1002/2015GC006048

Colgan, J.P., Egger, A.E., John, D.A., Cousens, B., Fleck, R.J. & Henry, C.D. 2011. Oligocene and Miocene arc volcanism in northeastern California: Evidence for post–Eocene segmentation of the subducting Farallon Plate. Geosphere: 7(3): 733–755. https://doi.org/10.1130/GES00650.1

Corredor, F. 2003. Seismic strain rates and distributed continental deformation in the northern Andes and three–dimensional seismotectonics of northwestern South America. Tectonophysics, 372(3–4): 147–166. https://doi.org/10.1016/S0040-1951(03)00276-2

Cortés, M. & Angelier, J. 2005. Current states of stress in the northern Andes as indicated by focal mechanisms of earthquakes. Tectonophysics, 403(1–4): 29–58. https://doi.org/10.1016/j.tecto.2005.03.020

Dyment, J., Lesur, V., Hamoudi, M., Choi, Y., Thebault, E. & Catalan, M. 2015. World digital magnetic anomaly map version 2.0. http://www.wdmam.org (consulted in October 2017).

Egbue, O. & Kellogg, J. 2010. Pleistocene to present North Andean "escape". Tectonophysics, 489(1–4): 248–257. https://doi.org/10.1016/j.tecto.2010.04.021

Ekström, G., Nettles, M. & Dziewoński, A.M. 2012. The global CMT project 2004–2010: Centroid–moment tensors for 13 017 earthquakes. Physics of the Earth and Planetary Interiors, 200–201: 1–9. https://doi.org/10.1016/j.pepi.2012.04.002

Frohlich, C. 2006. Deep earthquakes. Cambridge University Press, 574 p. New York.

Frohlich, C., Kadinsky–Cade, K. & Davis, S.D. 1995. A reexamination of the Bucaramanga, Colombia, earthquake nest. Bulletin of the Seismological Society of America, 85(6): 1622–1634.

Gómez, E., Jordan, T.E., Allmendinger, R.W., Hegarty, K., Kelly, S. & Heizler, M. 2003. Controls on architecture of the late Cretaceous to Cenozoic southern Middle Magdalena Valley Basin, Colombia. Geological Society of America Bulletin, 115(2): 131–147. https://doi.org/10.1130/0016-7606(2003)115<0131:-COAOTL>2.0.CO;2

Gutscher, M.A & Westbrook, G.K. 2009. Great earthquakes in slow–subduction, low–taper margins. In: Lallemand, S. & Funiciello, F. (editors), Subduction zone geodynamics, p. 119–133. https://doi.org/10.1007/978-3-540-87974-9

Hasegawa, A. & Nakajima, J. 2017. Seismic imaging of slab metamorphism and genesis of intermediate–depth intraslab earthquakes. Progress in Earth and Planetary Science, 4(12): 1–31. https://doi.org/10.1186/s40645-017-0126-9

Horton, B.K. 2018. Tectonic regimes of the central and southern Andes: Responses to variations in plate coupling during subduction. Tectonics, 37(2): 402–429. https://doi.org/10.1002/2017TC004624

Hunt, C.P., Moskowitz, B.M. & Banerjee, S.K. 1995. Magnetic properties of rocks and minerals. In: Ahrens, T.J. (editor), Rock physics & phase relations. A handbook of physical constants 3, p. 189–204. https://doi.org/10.1029/RF003p0189

Ibañez–Mejia, M., Tassinari, C.C.G. & Jaramillo–Mejía, J.M. 2007. U–Pb zircon ages of the "Antioquian Batholith": Geochronological constraints of late Cretaceous magmatism in the central Andes of Colombia. XI Congreso Colombiano de Geología. Abstracts, 11 p. Bucaramanga.

Idárraga–García, J., Kendall, J.M. & Vargas, C.A. 2016. Shear wave anisotropy in northwestern South America and its link to the Caribbean and Nazca subduction geodynamics. Geochemistry, Geophysics, Geosystems, 17(9): 3655–3673. https://doi.org/10.1002/2016GC006323

Keppie, D.F. 2014. The analysis of diffuse triple junction zones in plate tectonics and the pirate model of western Caribbean tectonics. SpringerBriefs in Earth Sciences, 75 p. New York. https://doi.org/10.1007/978-1-4614-9616-8

Kerr, A.C. & Tarney, J. 2005. Tectonic evolution of the Caribbean and northwestern South America: The case for accretion of two late Cretaceous oceanic plateaus. Geology, 33(4): 269–272. https://doi.org/10.1130/G21109.1

Koulakov, I. 2009. LOTOS code for local earthquake tomographic inversion: Benchmarks for testing tomographic algorithms. Bulletin of the Seismological Society of America, 99(1): 194–214. https://doi.org/10.1785/0120080013

Koulakov, I., Gordeev, E.I., Dobretsov, N.L., Vernikovsky, V.A., Senyukov, S., Jakovlev, A. & Jaxybulatov, K. 2013. Rapid

changes in magma storage beneath the Klyuchevskoy group of volcanoes inferred from time–dependent seismic tomography. Journal of Volcanology and Geothermal Research, 263: 75–91. https://doi.org/10.1016/j.jvolgeores.2012.10.014

Lara, M., Cardona, A., Monsalve, G., Yarce, J., Montes, C., Valencia, V., Weber, M., De la Parra, F., Espitia, D. & López–Martínez, M. 2013. Middle Miocene near trench volcanism in northern Colombia: A record of slab tearing due to the simultaneous subduction of the Caribbean Plate under South and Central America? Journal of South American Earth Sciences, 45: 24–41. https://doi.org/10.1016/j.jsames.2012.12.006

Lay, T. & Wallace, T.C. 1995. Modern global seismology. Academic Press, 517 p.

Lonsdale, P. 2005. Creation of the Cocos and Nazca plates by fission of the Farallon Plate. Tectonophysics, 404(3–4): 237–264. https://doi.org/10.1016/j.tecto.2005.05.011

Mantilla–Figueroa, L.C., Mendoza, H., Bissig, T. & Craig, H. 2011. Nuevas evidencias sobre el magmatismo miocénico en el distrito minero de Vetas–California (Macizo de Santander, cordillera Oriental, Colombia). Boletín de Geología, 33(1): 43–58.

Masy, J., Niu, F., Levander, A., & Schmitz, M. 2015. Lithospheric expression of Cenozoic subduction, Mesozoic rifting and the Precambrian Shield in Venezuela. Earth and Planetary Science Letters, 410: 12–24. http://doi.org/10.1016/j.epsl.2014.08.041

Mazuera–Rico, F. 2018. Estructura litosférica de la Cuenca de Falcón, región nororiental de los Andes de Mérida y Macizo El Baúl, Venezuela, a partir de perfiles sísmicos profundos. Doctoral thesis, Universidad Central de Venezuela. Caracas.

Michael, A.J., Ellsworth, W.L. & Oppenheimer, D.H. 1990. Coseismic stress changes induced by the 1989 Loma Prieta, California earthquake. Geophysical Research Letters, 17(9): 1441–1444. https://doi.org/10.1029/GL017i009p01441

Mora, A., Parra, M., Rodríguez–Forero, G., Blanco, V., Moreno, N.R., Caballero, V., Stockli, D.F., Duddy, I.R. & Ghorbal, B. 2015. What drives orogenic asymmetry in the northern Andes?: A case study from the apex of the northern Andean orocline. In: Bartolini, C. & Mann, P. (editors), Petroleum geology and potential of the Colombian Caribbean margin. American Association of Petroleum Geologists, Memoir 108, p. 547–586. https://doi.org/10.1306/13531949M1083652

Mora–Páez, H., Kellogg, J.N. & Freymueller, J.T. 2020. Contributions of space geodesy for geodynamic studies in Colombia: 1988 to 2017. In: Gómez, J. & Pinilla–Pachon, A.O. (editors), The Geology of Colombia, Volume 4 Quaternary. Servicio Geológico Colombiano, Publicaciones Geológicas Especiales 38, p. 479–498. Bogotá. https://doi.org/10.32685/pub.esp.38.2019.14

Mosquera–Machado, S., Lalinde–Pulido, C., Salcedo–Hurtado, E. & Michetti, A.M. 2009. Ground effects of the 18 October 1992, Murindó earthquake (NW Colombia), using the environmental seismic intensity scale (ESI 2007) for the assessment of intensity. In: Reicherter, K., Michetti, A.M. & Silva, P.G. (editors), Palaeoseismology: Historical and prehistorical records of earthquake ground effects for seismic hazard assessment. Geological Society of London, Special Publication 316, p. 123–144. https://doi.org/10.1144/SP316.7

Ojeda, A. & Havskov, J. 2001. Crustal structure and local seismicity in Colombia. Journal of Seismology, 5(4): 575–593. https://doi.org/10.1023/A:1012053206408

Okubo, Y. & Matsunaga, T. 1994. Curie point depth in northeast Japan and its correlation with regional thermal structure and seismicity. Journal of Geophysical Research Solid Earth, 99(B11): 22363–22371. https://doi.org/10.1029/94JB01336

Okubo, Y., Graf, R.J., Hansen, R.O., Ogawa, K. & Tsu, H. 1985. Curie point depths of the island of Kyushu and surrounding areas, Japan. Geophysics, 50(3): 481–494. https://doi.org/10.1190/1.1441926

Ordóñez–Carmona, O., Martins, M. & Ángel, P. 2001. Consideraciones geocronológicas e isotópicas preliminares del magmatismo Cretáceo–Paleoceno en el norte de la cordillera Central. VIII Congreso Colombiano de Geología. Memoirs, 5 p. Manizales.

Ottemöller, L., Voss, P. & Havskov, J. 2016. Seisan–earthquake analysis software for Windows, Solaris, Linux and MacosX, version 10.5: http://seisan.info (consulted in October 2017).

Parra, M., Mora, A., Sobel, E.R., Strecker, M.R. & González, R. 2009. Episodic orogenic front migration in the northern Andes: Constraints from low–temperature thermochronology in the Eastern Cordillera, Colombia. Tectonics, 28(4): 1–27. https://doi.org/10.1029/2008TC002423

Parra, M., Mora, A., López, C., Rojas, L.E. & Horton, B.K. 2012. Detecting earliest shortening and deformation advance in thrust–belt hinterlands: Example from the Colombian Andes. Geology, 40(2): 175–178. https://doi.org/10.1130/G32519.1

Paulatto, M., Laigle, M., Galve, A., Charvis, P., Sapin, M., Bayrakci, G., Evain, M. & Kopp, H. 2017. Dehydration of subducting slow–spread oceanic lithosphere in the Lesser Antilles. Nature Communications, 8(15980): 1–11. https://doi.org/10.1038/ncomms15980

Pavlis, N.K., Holmes, S.A., Kenyon, S.C. & Factor, J.K. 2012. The development and evaluation of the earth gravitational model 2008 (EGM2008). Journal of Geophysical Research Solid Earth, 117(B4): 1–38. https://doi.org/10.1029/2011JB008916

Pérez, O.J. & Mendoza, J.S. 1998. Sismicidad y tectónica en Venezuela y áreas vecinas. Física de la Tierra, 10: 87–110.

Poli, P., Prieto, G.A., Yu, C.Q., Flórez, M., Agurto–Detzel, H., Mikesell, T.D., Chen, G., Dionicio, V. & Pedraza, P. 2016. Complex rupture of the M6.3 2015 March 10 Bucaramanga earthquake: Evidence of strong weakening process. Geophysical Journal International, 205(2): 988–994. https://doi.org/10.1093/gji/ggw065

Poveda, E., Monsalve, G. & Vargas, C.A. 2015. Receiver functions and crustal structure of the northwestern Andean region, Colombia. Journal of Geophysical Research: Solid Earth, 120(4): 2408–2425. https://doi.org/10.1002/2014JB011304

Poveda, E., Julià, J., Schimmel, M. & Pérez–García, N. 2018. Upper and middle crustal velocity structure of the Colombian Andes

from ambient noise tomography: Investigating subduction–related magmatism in the overriding plate. Journal of Geophysical Research: Solid Earth, 123(2): 1459–1485. https://doi.org/10.1002/2017JB014688

Prieto, G.A., Beroza, G.C., Barrett, S.A., López, G.A. & Flórez, M. 2012. Earthquake nests as natural laboratories for the study of intermediate–depth earthquake mechanics. Tectonophysics, 570–571: 42–56. https://doi.org/10.1016/j.tecto.2012.07.019

Prieto, G.A., Flórez, M., Barrett, S.A., Beroza, G.C., Pedraza, P., Blanco, J.F. & Poveda, E. 2013. Seismic evidence for thermal runaway during intermediate–depth earthquake rupture. Geophysical Research Letters, 40(23): 6064–6068. https://doi.org/10.1002/2013GL058109

Quinteros, C. 2007. Estudio del espesor de la corteza y caracterización de sus posibles discontinuidades en la región noroccidental de Venezuela, a partir del análisis de funciones receptoras. Bachelor thesis, Universidad Central de Venezuela, 195 p. Caracas.

Ramos, V. 2015. Prologue: Caribbean–South American interactions: New data and interpretations. In: Schmitz, M., Audermard, F.A. & Urbani, F. (editors), The northeastern limit of the South American Plate–lithospheric structures from surface to the mantle. Editorial Innovación Tecnológica, p. v–viii. Caracas.

Restrepo–Moreno, S.A., Foster, D.A., Stockli, D.F. & Parra–Sánchez, L.N. 2009. Long–term erosion and exhumation of the "Altiplano Antioqueño", northern Andes (Colombia) from apatite (U–Th)/He thermochronology. Earth and Planetary Science Letters, 278(1–2): 1–12. https://doi.org/10.1016/j.epsl.2008.09.037

Reyes–Harker, A., Ruiz–Valdivieso, C.F., Mora, A., Ramírez–Arias, J.C., Rodríguez, G., de la Parra, F., Caballero, V., Parra, M., Moreno, N., Horton, B.K., Saylor, J.E., Silva, A., Valencia, V., Stockli, D.F. & Blanco, V. 2015. Cenozoic paleogeography of the Andean foreland and retroarc hinterland of Colombia. American Association of Petroleum Geologists Bulletin, 99(8): 1407–1453. https://doi.org/10.1306/06181411110

Rosenbaum, G. & Mo, W. 2011. Tectonic and magmatic responses to the subduction of high bathymetric relief. Gondwana Research, 19(3): 571–582. https://doi.org/10.1016/j.gr.2010.10.007

Saeid, E., Bakioglu, K.B., Kellogg, J., Leier, A., Martínez, J.A. & Guerrero, E. 2017. Garzón Massif basement tectonics: Structural control on evolution of petroleum systems in upper Magdalena and Putumayo Basins, Colombia. Marine and Petroleum Geology, 88: 381–401. https://doi.org/10.1016/j.marpetgeo.2017.08.035

Salazar, J.M. & Vargas, C.A. 2015. Fractal dimension and seismotectonic deformation rates along an inter–plate setting: Seismic regime along the Caribbean Plate boundary zone. In: Bartolini, C. & Mann, P. (editors), Petroleum geology and potential of the Colombian Caribbean margin. American Association of Petroleum Geologists, Memoir 108, p. 271–294. https://doi.org/10.1306/13531940M1083644

Salazar, J.M., Vargas, C.A. & León, H. 2017. Curie point depth in the SW Caribbean using the radially averaged spectra of magnetic anomalies. Tectonophysics, 694: 400–413. https://doi.org/10.1016/j.tecto.2016.11.023

Schneider, J.F., Pennington, W.D. & Meyer, R.P. 1987. Microseismicity and focal mechanisms of the intermediate–depth Bucaramanga nest, Colombia. Journal of Geophysical Research: Solid Earth, 92(B13): 13913–13926. https://doi.org/10.1029/JB092iB13p13913

Syracuse, E.M., Maceira, M., Prieto, G.A., Zhang, H. & Ammon, C.J. 2016. Multiple plates subducting beneath Colombia, as illuminated by seismicity and velocity from the joint inversion of seismic and gravity data. Earth and Planetary Science Letters, 444: 139–149. https://doi.org/10.1016/j.epsl.2016.03.050

Taboada, A., Rivera, L.A., Fuenzalida, A., Cisternas, A., Philip, H., Bijwaard, H., Olaya, J. & Rivera, C. 2000. Geodynamics of the northern Andes: Subductions and intracontinental deformation (Colombia). Tectonics, 19(5): 787–813. https://doi.org/10.1029/2000TC900004

Trenkamp, R., Kellogg, J.N., Freymueller, J.T. & Mora, H. 2002. Wide plate margin deformation, southern Central America and northwestern South America, CASA GPS observations. Journal of South American Earth Sciences, 15(2): 157–171. https://doi.org/10.1016/S0895-9811(02)00018-4

van der Hilst, R.D. & Mann, P. 1994. Tectonic implications of tomographic images of subducted lithosphere beneath northwestern South America. Geology, 22(5): 451–454. https://doi.org/10.1130/0091-7613(1994)022<0451:TIOTIO>2.3.CO;2

Vargas, C.A. & Mann, P. 2013. Tearing and breaking off of subducted slabs as the result of collision of the Panama Arc–indenter with northwestern South America. Bulletin of the Seismological Society of America, 103(3): 2025–2046. https://doi.org/10.1785/0120120328

Vargas, C.A. & Torres, R. 2015. Three–dimensional velocity structure of the Galeras Volcano (Colombia) from passive local earthquake tomography. Journal of Volcanology and Geothermal Research, 301: 148–158. https://doi.org/10.1016/j.jvolgeores.2015.05.007

Vargas, C.A., Ugalde, A., Pujades, L.G. & Canas, J.A. 2004. Spatial variation of coda wave attenuation in northwestern Colombia. Geophysical Journal International, 158(2): 609–624. https://doi.org/10.1111/j.1365-246X.2004.02307.x

Vargas, C.A., Idárraga–García, J. & Salazar, J.M. 2015. Curie point depths in northwestern South America and the southwestern Caribbean Sea. In: Bartolini, C. & Mann, P. (editors), Petroleum geology and potential of the Colombian Caribbean margin. American Association of Petroleum Geologists, Memoir 108, p. 179–200. https://doi.org/10.1306/13531936M1083642

Veloza, G., Styron, R., Taylor, M. & Mora, A. 2012. Open–source archive of active faults for northwest South America. GSA Today, 22(10): 4–10. https://doi.org/10.1130/GSAT-G156A.1

Villagómez, D., Spikings, R., Mora, A., Guzmán, G., Ojeda, G., Cortés, E. & van der Lelij, R. 2011. Vertical tectonics at a continental crust–oceanic plateau plate boundary zone: Fission track thermochronology of the Sierra Nevada de Santa Marta, Colombia. Tectonics, 30(4): 1–18. https://doi.org/10.1029/2010TC002835

Waller II, T.D. & Frost, B.R. 2018. New Evidence for Spreading Ridge, Colombia Basin, Southern Caribbean. American Association of Petroleum Geologists, Hedberg Conference: Geology of Middle America–the Gulf of Mexico, Yucatan, Caribbean, Grenada and Tobago Basins and Their Margins, Abstracts, p. 117. Sigüenza, Spain.

Wiemer, S., McNutt, S.R. & Wyss, M. 1998. Temporal and three–dimensional spatial analysis of the frequency–magnitude distribution near Long Valley caldera, California. Geophysical Journal International, 134(2): 409–421. https://doi.org/10.1046/j.1365-246x.1998.00561.x

Zarifi, Z. 2006. Unusual subduction zones: Case studies in Colombia and Iran. Doctoral thesis, University of Bergen, 78 p. Bergen, Norway.

Explanation of Acronyms, Abbreviations, and Symbols:

CPD	Curie point depth	SCDB	South Caribbean deformed belt
PFZ	Panamá fracture zone	SMBF	Santa Marta–Bucaramanga Fault System
RSNC	Red Sismológica Nacional de Colombia	SMM	Santa Marta Massif

Author's Biographical Notes

Carlos Alberto VARGAS is a professor in the Universidad Nacional de Colombia in Bogotá. He is a geologist (Universidad de Caldas, 1993) and received an MS degree in physics (Universidad Tecnológica de Pereira, 1996), as well as MS and PhD degrees in earthquake engineering (Universitat Politècnica de Catalunya, 2003). He is dedicated to research in geodynamics, and his main interests currently are in subduction systems and their responses in sedimentary basins.